SIAM J. Applied Dynamical Systems
Vol. 19, No. 3, pp. 1758–1797

Parameterization Method for Unstable Manifolds of Standing Waves on the Line*

Blake Barker†, Jason Mireles James‡, and Jalen Morgan†

Abstract. We consider a linearly unstable standing wave solution of a parabolic partial differential equation (PDE) on the real line and develop a high order method for polynomial approximation of the local unstable manifold. The unstable manifold describes the breakdown of the nonlinear wave after the loss of stability. Our method is based on the parameterization method for invariant manifolds and studies an invariance equation describing a local chart map. This invariance equation is a PDE posed on the product of a disk and the line. The dimension of the disk is equal to the Morse index of the wave. We develop a formal series solution for the invariance equation, and show that the coefficients of the series solve certain boundary value problems (BVPs) on the line. We solve these BVPs numerically to any desired order. The result is a polynomial describing the dynamics of the PDE in a macroscopic neighborhood of the unstable standing wave. The method is implemented for a number of example problems. Truncation/numerical errors are quantified via a posteriori indicators.

Key words. traveling waves, unstable manifold, PDE on the line, parameterization method, formal series expansion, numerical methods

AMS subject classifications. 74J30, 34C45, 35B99, 35Q55, 65M99

DOI. 10.1137/19M128243X

1. Introduction.

Understanding the emergence and evolution of coherent structures is a fundamental challenge in applied mathematics, and a rich class of examples come from partial differential equations (PDEs) posed on the entire real line. Traveling waves are an important special class of solutions where one looks for a fixed wave profile propagating with fixed wave speed. Waves with zero speed are known as standing waves. Questions about the existence and qualitative properties of traveling waves for one dimensional PDEs are equivalent to questions about the existence and shape of certain homoclinic/heteroclinic connecting orbits for finite dimensional vector fields. This observation leads to a dramatic reduction in the dimension of the problem and forges deep connections between the theory of nonlinear waves and the qualitative theory of dynamical systems.

Given a particular nonlinear wave solution, a natural problem is to consider its stability. That is, what happens to patterns starting near the traveling wave? While stable waves are observed in a wide variety of natural systems and mathematical models, unstable waves are not attracting, hence, they are difficult to observe directly. Nevertheless, insights from the qualitative theory of dynamical systems suggest that unstable waves play an important

*Received by the editors August 20, 2019; accepted for publication (in revised form) by M. Beck May 20, 2020; published electronically July 28, 2020.
https://doi.org/10.1137/19M128243X
Funding: The work of the second author was partially supported by NSF grant DMS-1813501.

†Department of Mathematics, Brigham Young University, Provo, UT 84602 (blake@mathematics.byu.edu, jalen.morgan@byu.edu).
‡Department of Mathematical Sciences, Florida Atlantic University, Boca Raton, FL 33431 (j.mireles.james@gmail.com).

role in the organization of global dynamics. For example, changes in stability are important for understanding spontaneous emergence and bifurcations of patterns. Moreover, unstable orbits are dense in chaotic attractors and understanding them is important for understanding spatiotemporal complexity.

Numerical analysis of traveling waves is a growing field, and within the last decade a number of tools for computing unstable waves have been developed. See for example [1, 2, 3, 4]. In the present work, we use the numerical package STABLAB [5] to compute the traveling wave profile and to determine the location of zeros of the Evans function, which are the isolated eigenvalues of the linearized (about the wave) PDE problem. We also use this software for automatic derivation of finite difference methods, which was recently added to STABLAB to simulate the flow generated by the PDE. This is important for quantifying error bounds.

The present work concerns the natural next step of studying nonlinear instabilities associated with traveling waves. We develop a new computational framework for high order Taylor approximation of the unstable manifold. Our approach is based on the parameterization method of Cabré, Fontich, and de la Llave [6, 7, 8]. The parameterization method is a general functional analytic paradigm for studying invariant manifolds in many different settings. The method is constructive and leads to efficient and accurate numerics. The parameterization is not required to be the graph of a function over an eigenspace, hence the method can follow folds in the embedding. In addition to providing the embedding, the parameterization method also recovers explicitly the dynamics on the manifold.

Following the works just cited—which focus on manifolds attached to fixed points of infinite dimensional maps—the parameterization method has been extended by a number of authors to more general situations such as whiskered tori [9, 10, 11, 12, 13, 14, 15], quasi-periodic invariant manifolds in infinite dimensional problems [16, 17, 18], and to stable/unstable manifolds attached to periodic orbits of ordinary differential equations [15, 19, 20, 21, 22, 23] to cite only a few developments. We refer to the book [24] for a much more complete overview of the literature. We only mention that several recent papers develop numerical approximation schemes for unstable manifolds in infinite dimensional dynamical systems. See, for example, the work of [25] on unstable manifolds attached to equilibrium and periodic orbits of delay differential equations, the work of [26] on unstable manifolds attached to equilibrium solutions of one dimensional scalar parabolic PDEs posed on compact intervals, and the extension to planar polygonal domains using finite element methods [27].

The main goal of the work at hand is to develop a parameterization method for the unstable manifold attached to a traveling wave solution of a parabolic PDE posed on the line. This represents a substantial generalization of the earlier works [25, 26, 27], as in the present setting linearizing about the nonlinear wave results in an essential spectrum. In contrast, the approach of [26], which studied PDEs formulated on compact intervals, results in a problem which can be projected onto a countable basis of eigenfunctions—reducing to a system of countably many ordinary differential equations. For PDEs on the line there is no such basis. Instead we exploit dynamical systems techniques developed for studying nonlinear waves, where the standing wave (or more generally a traveling wave) is reformulated as a homoclinic (more generally a heteroclinic orbit) for an auxiliary system of ODEs.

We combine the classic geometric approach to nonlinear waves with the parameterization method. The program begins by studying an invariance equation describing a chart for the

local unstable manifold. We develop, in the context of a number of examples, formal series solutions for the invariance equation and show that the coefficients of the series are given by a recursive scheme. The main observation is that the recursive system of equations describing the Taylor series coefficients are themselves linear boundary value problems (BVPs)—the so-called homological equations—with each BVP again formulated on the line. These equations are amenable to the same geometric methods used to study the nonlinear wave itself, and numerically solving the recursive system up to some finite order N provides a polynomial approximation of the parameterization.

The parameterization conjugates the dynamics on the manifold to the linear dynamics given by the unstable eigenvalues. Checking the conjugacy provides an a posteriori measure of the truncation/numerical error. We implement the scheme for three systems with well-known unstable standing waves: the Nagumo equation, the Gray–Scott system, and a nonlinear Schrödinger's equation. We compute the manifold to high order and verify its accuracy using automatic finite difference code described in [28]. In addition, we perform an a posteriori error analysis of each calculation. The MATLAB code is freely available at github.com/nonlinear-waves/stablab_matlab/tree/master/Parameterization_Method

Before concluding this introduction we remark that numerical methods for computing invariant manifolds for PDEs and other infinite dimensional systems have a long history and rich literature. While a thorough review of the literature is far beyond the scope of the present work, we would like to mention—in addition to the references cited above—a few papers which could serve as an entry point to this vast literature. We refer for example to the works [29, 30, 31, 32] on heteroclinic and homoclinic phenomena, the works [33, 34, 35, 36, 37] for a description of the organizing role of unstable periodic orbits and their invariant manifolds in the study of turbulence, to the works [38, 39, 40, 41, 42] on numerical methods for inertial manifold reduction, the works [43, 44, 45, 46] on numerical methods for center manifold reduction, the works [47, 48, 49, 50, 51] on efficient numerical calculation of spectral submanifolds, and the work [52, 53, 54, 55, 56, 57] on the role of invariant manifolds in delay differential equations. Again, we stress that this list barely scratches the surface of the literature, and that the interested reader will find much of interest by consulting the references of the papers just mentioned.

Remark 1.1 (the main examples). Most of the explicit example problems considered in the present work result in standing waves, though an example of how to treat waves with nonzero speed is given in section 4.4. Restricting ourselves to standing waves is a minor simplification which allows us to demonstrate the method with several well-known problems where the wave profile and wave speed (which is zero) are explicitly known. As illustrated in section 3.1 the homological equations—and hence the formal calculation of the unstable manifold parameterization—for standing and traveling waves are nearly identical once the wave speed has been determined. That is, the difference between working with standing and traveling waves appears only at zeroth order. Numerical methods for computing traveling waves with nonzero wave speed are well established but somewhat off the main topic of the present work. For the sake of simplicity, we focus largely on examples involving standing waves.

Remark 1.2 (PDEs on an interval versus PDEs on the line). An alternative approach to that taken here would be to truncate $\mathbb{R}$ to an interval of the form $[-L, L]$ for $L > 0$ sufficiently large,

and then apply the numerical scheme developed in [26]. While in a particular application this might (or might not) result in acceptable numerical results, the proposed truncation represents a very singular perturbation and completely changes the spectrum of the linearized problem, and this truncation is often avoided even for the numerical calculation of the zeroth order term (the nonlinear traveling wave profile itself). Moreover, while the present work is not concerned with convergence of the formal series, one of the goals of the present work is to properly formulate the discussion of the unstable manifold parameterization on $\mathbb{R}$ in anticipation of future works in this direction.

The remainder of the paper is organized as follows. After reviewing some requisite background material and presenting the main example problems in section 2, we describe in section 3 the parameterization method for standing waves of PDEs on the line. We place a heavy emphasis on formal series solutions of the invariance equation for the main example applications—that is, we emphasize the derivation of the homological equations in concrete problems. In section 4 we describe and implement numerical procedures for solving the homological equations and profiling the results. Some conclusions and suggestions for future work are discussed in section 5.

2. Background.

We begin by reviewing some now standard results about the parameterization method. In particular the invariance equation is given and its basic implications discussed. This material comprises only a few pages and is included so that the present work may serve as a stand alone introduction to the reader unfamiliar with these developments.

Similarly we describe some classical material about computation and stability analysis of traveling wave solutions for PDEs on the line. This material underpins our entire approach. We conclude the section by presenting the three main example applications studied in this present work: Nagumo's equation, the Gray–Scott system, and a nonlinear Schrödinger equation. For each system we provide a nontrivial unstable standing wave solution for further analysis later in the paper.

The reader familiar with the topics reviewed in this section is encouraged to skip ahead to section 3. Indeed, many readers will want to skim the present section and refer back to it only as needed.

2.1. Overview of the parameterization method for unstable manifolds of vector fields.

Let $\mathcal{H}$ be a Hilbert space, $\mathcal{D} \subset \mathcal{H}$ be a dense subset. For a smooth mapping $\mathcal{F}\colon \mathcal{D} \to \mathcal{H}$ consider the differential equation

$$\frac{\partial}{\partial t} u(t) = \mathcal{F}(u(t)). \tag{1}$$

We are interested in the dynamics near an equilibrium solution $u_* \in \mathcal{D}$. Observe that u_* is an equilibrium solution if

$$\mathcal{F}(u_*) = 0.$$

Assume that $A = D\mathcal{F}(u_*)$ has a finite Morse index. More precisely, we require that A has at most finitely many unstable eigenvalues each with only finite multiplicity. We write $\lambda_1, \dots, \lambda_M$ to denote the unstable eigenvalues and order them so that

$$0 < \operatorname{real}(\lambda_1) \leq \cdots \leq \operatorname{real}(\lambda_M).$$

In the present work we assume for the sake of simplicity that each unstable eigenvalue has multiplicity one. This assumption can be removed (for example see [6, 58]); however, in the present work we avoid these technicalities. Choose $\xi_1, \dots, \xi_M \in \mathcal{H}$ associated eigenvectors. More precisely we require that

$$D\mathcal{F}(u_*)\xi_j = \lambda_j \xi_j, \qquad 1 \le j \le M.$$

If $M \ge 0$ the equilibrium u_* is said to be spectrally unstable, and we are interested in parameterization of the M dimensional unstable manifold attached to u_*. To be more precise, let $r_1, \dots, r_M > 0$ and define $\mathbb{B} = [-r_1, r_1] \cdots [-r_M, r_M]$. Consider a smooth function $P \colon \mathbb{B} \to \mathcal{H}$ having that

$$P(0) = u_*, \tag{2}$$

$$\partial_j P(0) = \xi_j, \qquad 1 \le j \le M. \tag{3}$$

Such a P is tangent to the unstable manifold, and we want that

$$P(\mathbb{B}) \subset W^u(u_*).$$

Write

$$\Lambda = \begin{pmatrix} \lambda_1 & \dots & 0 \\ \vdots & \ddots & \vdots \\ 0 & \dots & \lambda_M \end{pmatrix}.$$

The parameterization method looks for a P which, in addition to satisfying the constraint equations (2) and (3), is also a solution of the *invariance equation*

$$\mathcal{F}(P(\theta)) = DP(\theta)\Lambda\theta \qquad \text{for all } \theta \in \text{interior}(\mathbb{B}). \tag{4}$$

Figure 1 illuminates the meaning of (4), which is asking that the pushforward of the linear vector field Λ by DP matches the vector field $\mathcal{F}$ restricted to the image of P. Loosely speaking, since the two vector fields match on the image of P they must generate the same dynamics—with the dynamics generated by Λ well understood. Then P maps orbits of Λ in $\mathbb{B}$ to orbits of $\mathcal{F}$ on the image of P, as we will show below. Since P maps orbits to orbits, (4) is also called an infinitesimal conjugacy equation. The orbit correspondence is illustrated in Figure 2, and the observations of the preceding paragraph are made precise by the following lemma. For the sake of simplicity we suppose that the unstable eigenvalues are real. This restriction can be lifted and complex conjugate eigenvalues handled as described in [59], and we actually consider this case in section 2.3. The elementary proof of the lemma is found in [27].

Lemma 2.1 (Orbit correspondence). *Assume that the unstable eigenvalues $\lambda_1, \dots, \lambda_M$ are real and distinct. Suppose that $P \colon \mathbb{B} \to \mathcal{H}$ satisfies the first order constraints of (2) and (3), and that P is a smooth solution of (4) on interior$(\mathbb{B}) = (-r_1, r_1) \times \cdots \times (-r_M, r_M)$. Then P parameterizes a local unstable manifold for u_*.*

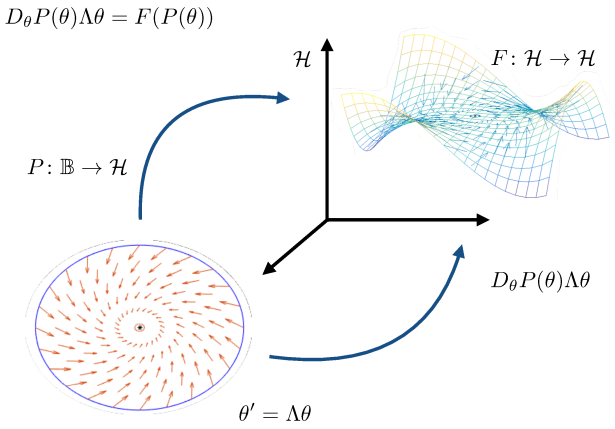

Figure 1. *Geometric interpretation of the invariance equation. $D_\theta P$ maps the vector field $\Lambda\theta$ in $\mathbb{B}$ onto the image of P. This pushforward should match that given vector field F in the image of P. If the two vector fields match then they generate the same dynamics (orbits).*

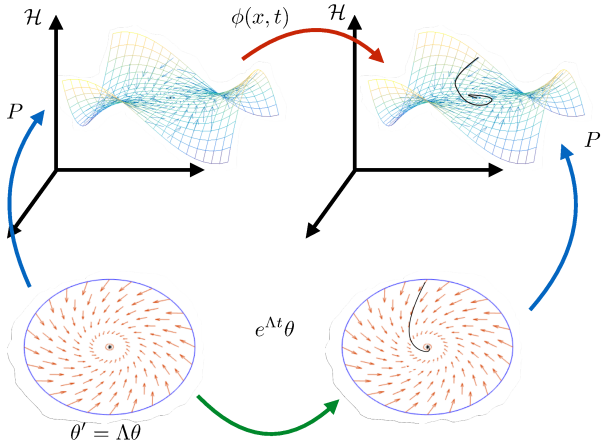

Figure 2. *Flow conjugacy induced by the invariance equation. The orbits of $e^{\Lambda t}$ accumulate in backwards time to the origin in $\mathbb{B}$. The parameterization P lifts these orbits to curves which are themselves orbits in $\mathcal{H}$. The orbits in $\mathcal{H}$ accumulate at the equilibrium u_*, so that the image of P is a local unstable manifold for u_* (4).*

Suppose that $\mathcal{F}$ generates a semiflow Φ in a neighborhood of u_*. In this case Lemma 2.1 can be restated by saying that P satisfies the flow conjugacy

$$P(e^{\Lambda t}\theta) = \Phi(P(\theta), t)$$

for all t such that $e^{\Lambda t}\theta \in \mathbb{B}$. So, P conjugates the flow generated by Λ to the flow generated by $\mathcal{F}$. In this sense, P recovers the dynamics on the parameterized manifold in addition to the embedding.

Lemma 2.1 explains our interest in the invariance equation (4). Sections 2.1 and 4, respectively, develop formal series methods for solving (4) as well as numerical implementation of the solutions.

2.2. Stability of traveling waves. This section reviews some basic material on traveling wave solutions of PDEs formulated on the real line. The material is standard and we do provide a citation for every relevant fact. We refer the reader to the excellent books [60, 61] for much more thorough discussions, including references to the primary literature.

Consider the parabolic PDE

$$\partial_t u = \partial_x^n u + N\left(u, \partial_x u, \partial_x^2 u, \dots, \partial_x^{n-1} u\right), \tag{5}$$

where $u\colon \mathbb{R} \times [0,\infty) \to \mathbb{R}$ and $N\colon \mathbb{R}^n \to \mathbb{R}$ are smooth functions. While the methods of the present work apply also to systems of PDEs (see the examples) we focus in this section on scalar equations to minimize technicalities.

A traveling wave solution of (5) is a function of the form

$$u(x,t) = u_*(x - ct),$$

where $u_*\colon \mathbb{R} \to \mathbb{R}$ is called the wave profile. We ask that u_* be a smooth, bounded function, with n bounded derivatives. The number $c \in \mathbb{R}$ is called the wave speed of the traveling wave. If $c = 0$ then u_* is a standing wave.

Making the change of variables $s = x - ct$ we see that the function u_* solves the ordinary differential equation (ODE)

$$\frac{d^n}{ds^n} u + cu' + N\left(u, u'', \dots, \frac{d^{n-1}}{ds^{n-1}} u\right) = 0. \tag{6}$$

We focus on traveling waves with simple behavior at infinity. In particular, if

$$\lim_{s\to-\infty} u_*(s) = a_-, \qquad \text{and} \qquad \lim_{s\to\infty} u_*(s) = a_+, \tag{7}$$

then we say that $u(x,t) = u_*(x - ct)$ is a traveling front. If $a_- = a_+$, it is a traveling pulse.

Introducing the variables $U = (u_1, \dots, u_n)$, where

$$u_1 = u, \quad u_2 = u', \quad \dots, \quad u_n = \frac{d^{n-1}}{ds^{n-1}} u,$$

allows us to rewrite (6) as a one parameter family of vector fields

$$U' = F_c(U)$$

with

$$F_c(U) = F(U,c) = F(u_1, \dots, u_n, c) = \begin{pmatrix} u_2 \\ u_3 \\ \vdots \\ u_n \\ -cu_2 - N(u_1, \dots, u_n) \end{pmatrix}.$$

The vector $a \in \mathbb{R}^n$ is an equilibrium solution of the vector field if and only if

$$F_c(a) = 0.$$

Referring back to the explicit formula for F_c we see that a is an equilibrium solution if and only if

$$a_2 = a_3 = \cdots = a_n = 0,$$

and

$$-ca_2 - N(a_1, a_2, \ldots, a_{n-1}, a_n) = -N(a_1, 0, \ldots, 0, 0) = 0.$$

So, the possible asymptotic values for traveling fronts and pulses are given by the roots of the function $g(x) = N(x, \ldots, 0, 0)$.

Suppose that $a_\pm$ are a pair of roots of $g(x)$. The question "*does there exist a traveling front/pulse with wave speed c and asymptotic limits* $a_\pm$*?*" is equivalent to the question "*does there exist a heteroclinic/homoclinic orbit for the vector field* F_c *from the equilibrium* $U_- = (a_-, 0, \ldots, 0)$ *to the equilibrium* $U_+ = (a_+, 0, \ldots, 0)$*?*" The answer to the later question is *yes* if the unstable manifold of U_- intersects the stable manifold of U_+. Then it is natural to require that $U_\pm$ are hyperbolic.

Indeed, let i_+ denote the number of unstable eigenvalues of $DF_c(U_+)$ and i_- denote the number of stable eigenvalues of $DF_c(U_-)$. If U_+ and U_- are distinct, and $i_+ + i_- = n+1$, then it is possible for the unstable manifold of U_+ to intersect transversally the stable manifold of U_-. In this case there is an isolated connecting orbit from U_+ to U_- and, hence, an isolated traveling wave solution of the PDE for an open set of parameters c. If, on the other hand, $i_- + i_+ = n$ (where $U_\pm$ may or may not be distinct) then the stable/unstable manifolds cannot intersect transversally, and isolated connections are a codimension one phenomenon occurring at isolated parameter values c. This provides a geometric mechanism for selecting the wave speed.

Since the wave profile is a component function of a heteroclinic/homoclinic connection between hyperbolic equilibrium solutions of an ODE, the convergence to constant asymptotic behavior is exponential. More precisely, there is an $r > 0$ so that

$$\lim_{x \to -\infty} e^{r|x|} |u_*(x) - a_-| = 0 \qquad \text{and} \qquad \lim_{x \to \infty} e^{rx} |u_*(x) - a_+| = 0. \tag{8}$$

In the present work we study the existence of heteroclinic/homoclinic solutions on a case by case basis either from a numerical point of view or referring to standard known solutions from the literature.

Suppose now that $u_* \colon \mathbb{R} \to \mathbb{R}$ is a smooth traveling wave with exponential decay as in (8). We are interested in the behavior of solutions of (5) in a small neighborhood of u_*. Writing

$$u(x,t) = u_*(x) + h(x,t),$$

in (5) leads to

$$\begin{aligned}\partial_t h &= \partial_x^n h + ch' + N\left(u_* + h, \partial_x u_* + \partial_x h, \partial_x^2 u_* + \partial_x^2 h, \dots, \partial_x^{n-1} u_* + \partial_x^{n-1} h\right) \\ &= \partial_x^n h + ch' + \nabla N\left(u_*, \partial_x u_*, \partial_x^2 u_*, \dots, \partial_x^{n-1} u_*\right) \begin{pmatrix} h \\ \partial_x h \\ \dots \\ \partial_x^{n-1} h \end{pmatrix} + R_{u_*}\left(h, \partial_x h, \dots, \partial_x^{n-1} h\right) \\ &= \mathcal{F}(h), \end{aligned} \tag{9}$$

where $\mathcal{F}$ is now an evolution equation of the form (1). Indeed, under mild assumptions to be specified below, $\mathcal{F}$ is a densely defined vector field on an appropriate Hilbert space.

Let

$$\begin{aligned} a_0 &= \partial_1 N(u_*, \partial_x u_*, \partial_x^2 u_*, \dots, \partial_x^{n-1} u_*), \\ a_1 &= \partial_2 N(u_*, \partial_x u_*, \partial_x^2 u_*, \dots, \partial_x^{n-1} u_*), \\ &\vdots \\ a_{n-1} &= \partial_n N(u_*, \partial_x u_*, \partial_x^2 u_*, \dots, \partial_x^{n-1} u_*), \end{aligned}$$

and note that the a_j for $0 \le j \le n$ are smooth bounded functions as N depends smoothly on u_* and its derivatives. In particular $a_j \in L^\infty(\mathbb{R})$ for $0 \le j \le n$. Moreover, defining the constants

$$a_j^{\pm} = \lim_{x \to \pm\infty} a_j(x),$$

we have that

$$\lim_{x \to \pm\infty} e^{r|x|} |a_j(x) - a_j^{\pm}| = 0$$

for some $r > 0$. That is, the $a_j(x)$, $0 \le j \le n$, are exponentially asymptotically constant.

We consider (9) as an evolution equation on $H^n(\mathbb{R})$, and note that the nonlinear stability of the origin in (9) is equivalent to the nonlinear stability of the traveling wave u_*. Under the mild assumptions on the coefficients a_j, $0 \le j \le n$, appearing below, the spectral mapping theorem implies that nonlinear stability of the trivial solution of (9) is determined by the spectral stability of the linear equation

$$\frac{\partial}{\partial t} h = \mathcal{L} h. \tag{10}$$

Here $\mathcal{L}\colon H^n(\mathbb{R}) \to L^2(\mathbb{R})$ is the closed, densely defined, exponentially asymptotic PDE

$$\mathcal{L} = \partial_x^n + c + a_0(x) + a_1(x)\partial_x + a_2(x)\partial_x^2 + \cdots + a_{n-1}(x)\partial_x^{n-1}. \tag{11}$$

Then the main question is to understand the spectrum of $\mathcal{L}$, and the analysis is complicated by the fact that $\mathcal{L}$ will typically have an essential spectrum.

Nevertheless, for a large class of equations the spectrum of $\mathcal{L}$ can be determined using standard techniques. The analysis exploits the fact that the operator is asymptotically constant. Define the constant coefficient linear differential operators

$$\mathcal{L}_+ = \partial_x^n + c + a_0^+ + a_1^+\partial_x + a_2^+\partial_x^2 + \cdots + a_{n-1}^+\partial_x^{n-1}$$

and

$$\mathcal{L}_- = \partial_x^n + c + a_0^- + a_1^-\partial_x + a_2^-\partial_x^2 + \cdots + a_{n-1}^-\partial_x^{n-1}.$$

The essential spectra of $\mathcal{L}_\pm$ can be worked out using Fourier transform methods. This results in two curves in the complex plane, the so called Fredholm boundary of $\mathcal{L}$. The essential spectrum of $\mathcal{L}$ is the region in $\mathbb{C}$ bound between these Fredholm boundaries. In particular, if $\mathcal{L}_\pm$ have an essential spectrum in the open left half-plane then so does $\mathcal{L}$.

We now clarify the necessary assumptions required for the spectral mapping theorem. These assumptions are satisfied by all the examples considered in the present work.

- A1: The essential spectrum of $\mathcal{L}$ is a subset of the open left half-plane.
- A2: The operator $\mathcal{L}$ has only finitely many isolated unstable eigenvalues, each with finite multiplicity.
- A3: The only zero eigenvalues are due to symmetries in the PDE and the associated eigenvectors are obtained by studying the symmetry group. In this case zero eigenvalues due to symmetries can be moved into the left-half plane using exponentially weighted norms.
- A4: The operator $\mathcal{L}$ generates an analytic semigroup.
- A5: The operator $\mathcal{N}\colon H^n(\mathbb{R}) \to H^n(\mathbb{R})$ defined by the Taylor remainder

  $$\mathcal{N}(h) = R_{u_*}(h),$$

  satisfies a quadratic estimate of the form

  $$\|N(h)\|_{H^n(\mathbb{R})} \leq C\|h\|_{H^n(\mathbb{R})}$$

  for some $C > 0$.

By A2 $\mathcal{L}$ has at most a finite number of eigenvalues in the open right half of the complex plane. These are the unstable eigenvalues. Under these assumptions it is possible to define the variation of constants formula, also known as Duhamel's principle, using the semigroup of A4. Then one can prove spectral mapping theorems (spectral stability implies nonlinear stability) as well as stable/unstable/center manifold theorems. In the context of the present work the essential point is that the unstable manifold has the same dimension as the number of unstable eigenvalues counted with multiplicity. That is, the unstable manifold is finite dimensional and we are in the situation described in section 2.1.

The isolated eigenvalues of $\mathcal{L}$ and, in particular the unstable spectrum, can be computed using the Evans function. We sketch the main ideas. Suppose that $\lambda \in \mathbb{C}$ and $\xi \in H^n(\mathbb{R})$. Then (λ, ξ) is an eigenvalue/eigenvector pair for $\mathcal{L}$ if

$$\mathcal{L}\xi = \lambda\xi,$$

which is

$$\frac{d^n}{dx^n}\xi + a_0(x)\xi + a_1(x)\xi' + a_2(x)\xi'' + \cdots + a_{n-1}(x)\frac{d^{n-1}}{dx^{n-1}}\xi = \lambda\xi.$$

A necessary condition for $\xi \in H^n(\mathbb{R})$ is that

$$\lim_{x\to\pm\infty} \xi(x) = 0.$$

As in the case of a traveling wave, the geometry of the eigenvalue problem is illuminated if we it rewrite as a system of ODEs. Let $Y = (y_1, \ldots, y_n)$ by $y_1 = \xi$, $y_2 = \xi', \ldots, y_n = d^{n-1}/dx^{n-1}$ and define the one parameter family of nonconstant coefficient linear systems

$$Y' = A(x,\lambda)Y,$$

where

$$A(x,\lambda) = \begin{pmatrix} 0 & 1 & 0 & \dots & 0 & 0 \\ 0 & 0 & 1 & \dots & 0 & 0 \\ \vdots & \vdots & \vdots & \ddots & \vdots & \vdots \\ 0 & 0 & 0 & \dots & 1 & 0 \\ 0 & 0 & 0 & \dots & 0 & 1 \\ \lambda - a_0(x) & -a_1(x) & -a_2(x) & \dots & a_{n-2}(x) & a_{n-1}(x) \end{pmatrix}.$$

Defining the constant coefficient matrices

$$A_\pm(\lambda) = \lim_{x\to\pm\infty} A(x,\lambda),$$

we see that the linear system $Y' = A(x,\lambda)Y$ is an asymptotically constant coefficient. Let $i_-(\lambda)$ and $i_+(\lambda)$ denote the Morse indices (number of unstable eigenvalues) of $A_-(\lambda)$ and $A_+(\lambda)$, and $\mathbb{E}^u_-(\lambda)$ and $\mathbb{E}^s_+(\lambda)$ denote the unstable and stable eigenspaces of $A_-(\lambda)$ and $A_+(\lambda)$, respectively. The eigenvalue problem for $\mathcal{L}$ is equivalent to solving the boundary value problem

$$Y' = A(x,\lambda)Y, \qquad \lim_{x\to\pm\infty} Y(x) \in \mathbb{E}^{s,u}_\pm(\lambda), \qquad Y \not\equiv 0. \tag{12}$$

By A2 there are only finitely many solutions of the problem, and the BVP can be solved numerically in explicit examples. When solving (12) numerically, λ is treated as a free parameter and a phase condition is imposed on the eigenfunction to select one solution among the family of nonzero multiples. A sufficiently good guess for the eigenvalue and eigenvector must be provided to the numerical solver. The Evans function can be used to obtain a good initial guess.

We briefly introduce the idea of the Evans function and refer the interested reader to the references, especially [60]. In the following discussion, we are restricting $\lambda \in \mathbb{C}$ to be to the right of the essential spectrum of $\mathcal{L}$. We let $Y^u_{-\infty}(x)$ be a matrix valued function whose columns form a basis, varying analytically in λ, for the set of solutions to

$$Y'(x) = A(x,\lambda)Y(x), \qquad \lim_{x\to-\infty} Y(x) \in \mathbb{E}^u_-(\lambda), \qquad Y \not\equiv 0,$$

and let $Y^s_{+\infty}(x)$ be a matrix valued function whose columns form a basis, also varying analytically in λ, for the set of solutions to

$$Y'(x) = A(x,\lambda)Y(x), \qquad \lim_{x\to+\infty} Y(x) \in \mathbb{E}^s_+(\lambda), \qquad Y \not\equiv 0.$$

The Evans function D is defined as the determinant of the concatenated matrix,

$$D(\lambda) := \det\left([Y^u_-(0), Y^s_+(0)]\right).$$

By construction, the Evans function is complex analytic and its zeros correspond to eigenvalues of $\mathcal{L}$. We may thus use complex analytic root finding techniques to locate the zeros of the Evans function. These provide good guesses for the eigenvalues, and $Y^s_{+\infty}(x)$ and $Y^u_{-\infty}(x)$ form good initial approximations of the associated eigenfunction.

We refer the interested reader to several additional papers about the Evans function, [60, 62, 63, 64, 65, 66, 67, 68, 69, 70, 71, 72, 73, 74, 75, 76, 77, 78, 79, 80, 81, 82, 83, 84, 85], though even this list is far from complete. Again, we remark that the STABLAB [5] software is used in the present work to compute wave profiles and zeros of the Evans function.

2.3. The main examples: Profiles and eigendata. In this section we describe the three models used in the present work. For each system we consider a standing wave profile and examine the stability via the Evans function. The first model is Nagumo's equation, for which an explicit pulse solution, explicit eigenvalue, and explicit eigenfunction are known. The second model, the Gray–Scott system, also has explicit solutions for unstable standing waves, but explicit solutions for its eigenfunctions are not known. The third system, Schrödinger's equation, is known to exhibit a Hopf bifurcation resulting in oscillating eigenfunctions associated with complex conjugate eigenvalues. The Gray–Scott and Schrödinger models illustrate that our method applies to systems as well as scalar equations. The Schrödinger model further illustrates the computation of a two dimensional unstable manifold.

2.3.1. Nagumo equation. The Nagumo equation in one spatial dimension is given by

$$u_t = u_{xx} - u + u^3, \tag{13}$$

where $u(x,t) : \mathbb{R}\times(0,\infty)\to\mathbb{R}$. The profile equation for a standing wave is

$$u'' - u + u^3 = 0,$$

which leads to the first order system

$$\begin{aligned} u_1' &= u_2, \\ u_2' &= u_1 - u_1^3. \end{aligned}$$

The Nagumo equation has an unstable standing wave solution given by

$$u_*(x) = u_1(x) = \sqrt{2}\,\operatorname{sech}(x).$$

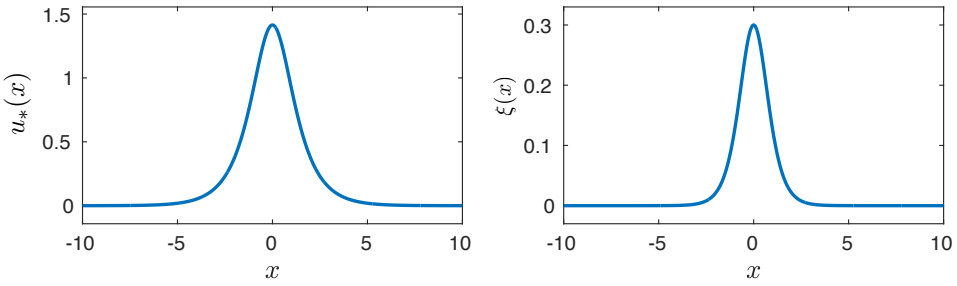

Figure 3. *The Nagumo equation profile, $u_*(x)$, and eigenfunction, $\xi(x)$, associated with the unstable eigenvalue $\lambda = 3$.*

Linearizing (13) about the wave u_* and looking for separated solutions (that is, ignoring the continuous spectrum) yields the eigenvalue problem

$$\xi''(x) - \xi(x) + 3u_*(x)^2\xi(x) = \lambda\xi(x), \quad \lim_{x\to\pm\infty} \xi(x) = 0, \quad ||\xi|| \neq 0. \tag{14}$$

A solution to (14) for the unique unstable eigenvalue $\lambda = 3$ is given by the eigenfunction

$$\xi(x) = \begin{cases} e^{2x}(2 - 2\tanh(x) - \operatorname{sech}^2(x)) & \text{if } x \geq 0, \\ e^{-2x}(2 + 2\tanh(x) - \operatorname{sech}^2(x)) & \text{if } x < 0, \end{cases}$$

can be seen in Figure 3. The profile and eigenfunction for Nagumo's equation are plotted in Figure 3.

2.3.2. Gray–Scott. The Gray–Scott equations in one spatial dimension are given by

$$\begin{aligned} u_t &= u_{xx} - uv^2 + \alpha(1-u), \\ v_t &= v_{xx} + uv^2/\gamma - v/\gamma, \end{aligned} \tag{15}$$

where $u, v : \mathbb{R} \times (0,\infty) \to \mathbb{R}$, and $\alpha, \gamma > 0$ are parameters. The equations model a cubic autocatalytic reaction without stirring [86, 87, 88]. The profile equations for a standing wave solution are

$$u'' = uv^2 - \alpha(1-u), \quad v'' = \frac{1}{\gamma}(v - uv^2). \tag{16}$$

We take $\alpha\gamma = 1$ and $0 < \gamma < \frac{2}{9}$, as for these parameters there is a known explicit solution (see [87]) for the profile equations given by

$$\begin{aligned} u_*(x) &= 1 - \frac{3\gamma}{1 + Q\cosh(x/\sqrt{\gamma})}, \\ v_*(x) &= \frac{3}{1 + Q\cosh(x/\sqrt{\gamma})}, \end{aligned} \tag{17}$$

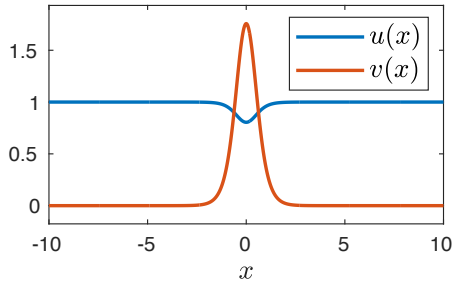

Figure 4. *Standing wave solution for the Gray–Scott equations.*

where $Q := \sqrt{1 - 9\gamma/2}$. These solutions were shown to be unstable in [89]. We select values of $\alpha = 9$ and $\gamma = \frac{1}{9}$. The corresponding profile is shown in Figure 4.

Linearizing (15) about the profile (u_*, v_*), and looking for separated solutions, we arrive at the eigenvalue problem

$$\xi'' - v_*^2\xi - 2u_*v_*\eta - \alpha\xi = \lambda\xi,$$
$$\eta'' + \frac{v_*^2}{\gamma}\xi + \frac{2}{\gamma}u_*v_*\eta - \frac{1}{\gamma}\eta = \lambda\eta,$$

which upon rearranging terms becomes the second order system

$$\xi'' = v_*^2\xi + 2u_*v_*\eta + \alpha\xi + \lambda\xi, \tag{18}$$

$$\eta'' = -\frac{v_*^2}{\gamma}\xi - \frac{2}{\gamma}u_*v_*\eta + \frac{1}{\gamma}\eta + \lambda\eta. \tag{19}$$

We note that, due to the symmetry of u_* and v_*, eigenfunctions may be even or odd functions of $x \in \mathbb{R}$. We introduce the variables $\xi_1 = \xi, \xi_2 = \xi', \eta_1 = \eta, \eta_2 = \eta'$ and write (18) as a first order system $W'(x;\lambda) = A(x;\lambda)W(x;\lambda)$ as follows:

$$\begin{pmatrix} \xi_1' \\ \xi_2' \\ \eta_1' \\ \eta_2' \end{pmatrix} = \begin{pmatrix} 0 & 1 & 0 & 0 \\ \lambda + v_*^2 + \alpha & 0 & 2u_*v_* & 0 \\ 0 & 0 & 0 & 1 \\ -v_*^2/\gamma & 0 & \lambda + (1 - 2u_*v_*)/\gamma & 0 \end{pmatrix} \begin{pmatrix} \xi_1 \\ \xi_2 \\ \eta_1 \\ \eta_2 \end{pmatrix}. \tag{20}$$

The asymptotic matrices $A_\pm := \lim_{x\to\pm\infty} A(x;\lambda)$ are given by

$$A_\pm(\lambda) = \begin{pmatrix} 0 & 1 & 0 & 0 \\ \lambda + \alpha & 0 & 0 & 0 \\ 0 & 0 & 0 & 1 \\ 0 & 0 & \lambda + 1/\gamma & 0 \end{pmatrix}. \tag{21}$$

The eigenvalues of $A_\pm$ are given by $\mu_1^\pm = \pm\sqrt{\lambda + \alpha}$ and $\mu_2^\pm = \pm\sqrt{\lambda + 1/\gamma}$. The associated eigenvectors are given by $v_1^\pm = (1, \mu_1^\pm, 0, 0)^T$ and $v_2^\pm = (0, 0, 1, \mu_2^\pm)^T$. Using these eigenvectors to create projective boundary conditions, we solve for the eigenfunctions as described at the end of section 2.2. The profiles of the eigenfunctions are illustrated in Figure 5.

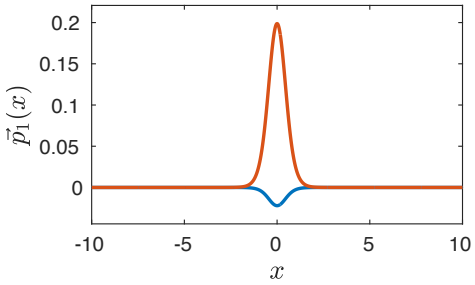

Figure 5. *The Gray–Scott eigenfunctions, $\xi(x)$ and $\eta(x)$ – red (top) and blue (bottom), respectively.*

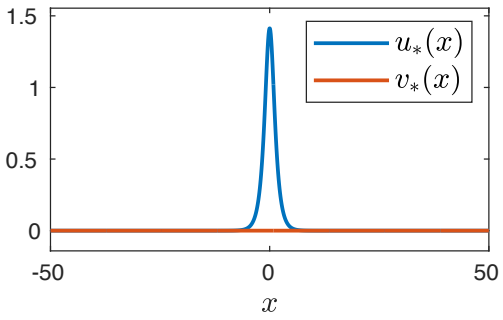

Figure 6. *Profile for PNLS. The blue (top) line corresponds to the component u_*, and the orange (bottom) line to the component v_*.*

2.3.3. Nonlinear Schrödinger equations. The rescaled, parametrically forced nonlinear Schrödinger equation (PNLS) in one spatial dimension is given by

$$\begin{aligned} u_t &= -v_{xx} + \mu v - v(v^2 + u^2), \\ v_t &= u_{xx} - u + u(v^2 + u^2) - 2\nu v, \end{aligned} \tag{22}$$

where u and v represent, respectively, the real and imaginary part of the dependent variable of the rescaled PNLS, and μ and ν are rescaled coefficients; see [90] for details. It was shown in [90] that Hopf bifurcations of a pulse solution exist in PNLS.

The system has a stationary pulse equilibrium given by $(u_*, v_*) = (\sqrt{2}\,\mathrm{sech}(x), 0)$ solving the profile equation

$$\begin{aligned} -v'' + \mu v - v^3 - vu^2 &= 0, \\ u'' - u - 2\nu v + uv^2 + u^3 &= 0; \end{aligned} \tag{23}$$

see Figure 6.

Linearizing about the profile leads to the eigenvalue problem

$$\begin{aligned} -\eta'' + \mu\eta - 3v_*^2\eta - u_*^2\eta - 2u_*v_*\xi &= \lambda\xi, \\ \xi'' - \xi - 2\nu\eta + v_*^2\xi + 2u_*v_*\eta + 3u_*^2\xi &= \lambda\eta. \end{aligned} \tag{24}$$

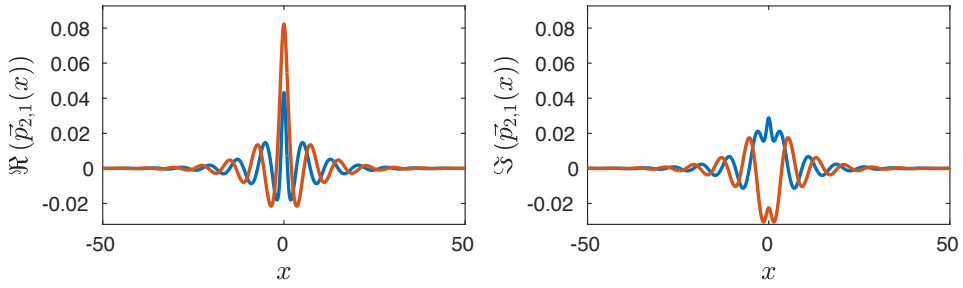

Figure 7. *The real and imaginary part of the eigenfunctions corresponding to the complex conjugate pair of eigenvalues* $\lambda_{1,2} = 0.0557 \pm 1.3053i$. *Red corresponds to* $\xi(x)$ *and blue to* $\eta(x)$.

We fix parameters $\mu = 0.3957$ and $\nu = 0.1745$, which correspond to $a = 4$ and $\gamma = 2$ in [90]. We solve for one of the eigenvalue-eigenfunction pairs of PNLS using the method described at the end of section 2.2, and then we obtain the other eigenpair by taking the complex conjugate of the first. These are a pair of complex conjugate unstable eigenvalues $\lambda_{1,2} \approx 0.0557 \pm 1.3053i$. We plot the real and imaginary parts of the associated eigenfunctions in Figure 7.

3. Unstable manifolds for standing waves: Formal series calculations.

In this section, we derive the formal derivation of the homological equations.

3.1. Homological equations for standing waves.

Suppose that $u_* \colon \mathbb{R} \to \mathbb{R}$ is a smooth traveling wave solution of (5). That is, we assume that u_* is an equilibrium solution of (9). Under assumptions A1–A5 there is a locally well-defined $L^2(\mathbb{R})$ flow near u_*, and the nonlinear stability of u_* is determined by spectral analysis of the asymptotically constant linearized problem. We assume that the linearized problem has m unstable eigenvalues each with multiplicity one, and we want to represent the local unstable manifold via the parameterization method. Let $\lambda_1, \ldots, \lambda_M \in \mathbb{C}$ denote the unstable eigenvalues and $\xi_1, \ldots, \xi_M \in H^n(\mathbb{R})$ an associated choice of eigenfunctions. Let Λ be the $M \times M$ diagonal matrix of unstable eigenvalues.

We look for a formal series approximation of the unstable manifold parameterization discussed in section 2.1, and make the power series ansatz

$$P(\theta_1, \ldots, \theta_M, x) = \sum_{m_1=0}^{\infty} \cdots \sum_{m_M=0}^{\infty} p_{m_1,\ldots,m_M}(x) \theta_1^{m_1} \ldots \theta_M^{m_M},$$

where $p_{m_1,\ldots,m_M} \in H^n(\mathbb{R})$ for $m_1 + \cdots + m_M \geq 1$. Observe that $p_{0,\ldots,0} = u_*$ and $p_{e_j} = \xi_j$ for $1 \leq j \leq M$. Note also that if

$$\sum_{m_1+\cdots+m_M \geq 1}^{\infty} \|p_{m_1,\ldots,m_M}\|_{H^n(\mathbb{R})} \, r_1^{m_1} \ldots r_M^{m_M} < \infty, \tag{25}$$

then, by a standard argument involving the monotone convergence theorem, we have that for

each $(\theta_1, \dots, \theta_M) \in (-r_1, r_1) \times \cdots \times (-r_M, r_M)$ the function $P(\theta_1, \dots, \theta_M, x)$ is in $u_* + H^n(\mathbb{R})$. Indeed, under the assumption given in (25) we have that $\tilde{P}\colon (-r_1, r_1) \times \cdots \times (-r_M, r_M) \to H^n(\mathbb{R})$ given by

$$\tilde{P} = P - u_*,$$

is a real analytic embedding of a disk.

Note that, on the level of formal power series, the differential operator on the left-hand side of (4) is expressed as

$$DP(\theta, x)\Lambda\theta = \sum_{m_1=0}^{\infty} \dots \sum_{m_M=0}^{\infty} (m_1\lambda_1 + \cdots + m_M\lambda_M)\, p_{m_1,\dots,m_M}(x)\theta_1^{m_1} \dots \theta_M^{m_M}.$$

Now write

$$\mathcal{F}(P(\theta, x)) = \sum_{m_1=0}^{\infty} \dots \sum_{m_M=0}^{\infty} q_{m_1,\dots,m_M}(x)\theta_1^{m_1} \dots \theta_M^{m_M},$$

where the power series coefficients $q_{m_1,\dots,m_M}$ depend on the power series coefficients of P in a problem specific manner. Matching like powers of $\theta = (\theta_1, \dots, \theta_M)$ leads to

$$(m_1\lambda_1 + \cdots + m_M\lambda_M)\, p_{m_1,\dots,m_M}(x) = q_{m_1,\dots,m_M}.$$

Indeed we will see, by considering the examples below, that

$$q_{m_1,\dots,m_M}(x) = D\mathcal{F}(u_*)p_{m_1,\dots,m_M}(x) + R_{m_1,\dots,m_M}(x), \tag{26}$$

where the functions $R_{m_1,\dots,m_M}\colon H^n(\mathbb{R}) \to L^2(\mathbb{R})$ depend only on lower order terms. That is, $R_{m_1,\dots,m_M}$ depends on coefficients $p_{j_1,\dots,j_M}$ with $j_1 < m_1, \dots, j_M < m_M$. The explicit form of the functions $R_{m_1,\dots,m_M}$ depend on the functional form of the nonlinearity of the traveling wave problem, and for the purposes of the present work we choose to work these out on a case by case basis. Nevertheless we remark that an explicit general formula for the $R_{m_1,\dots,m_M}$ (albeit one which is not especially computationally efficient) can be worked out using Faá di Bruno's formula. See, for example, [6].

Considering the definition of $\mathcal{F}$ in (9) and the definition of the linear operator $\mathcal{L}$ in (10), we have that

$$D\mathcal{F}(u_*)p_{m_1,\dots,m_M} = \mathcal{L}p_{m_1,\dots,m_M}$$

$$= \partial_x^n p_{m_1,\dots,m_M}(x) + cp_{m_1,\dots,m_M}(x) + a_0(x)p_{m_1,\dots,m_M}(x) + \cdots + a_{n-1}(x)\partial_x^{n-1}p_{m_1,\dots,m_M}(x).$$

That is

$$q_{m_1,\dots,m_M}(x) = \mathcal{L}p_{m_1,\dots,m_M} + R_{m_1,\dots,m_M}(x).$$

Returning to (26), we obtain that the *homological equation* defining $p_{m_1,\dots,m_M}(x)$ is given by the recursive system of asymptotically constant nth order linear BVPs on $\mathbb{R}$ defined by

$$\mathcal{L}p_{m_1,\dots,m_M}(x) - (m_1\lambda_1 + \cdots + m_M\lambda_M)p_{m_1,\dots,m_M}(x) = -R_{m_1,\dots,m_M}(x), \tag{27}$$

where $R_{m_1,\dots,m_M} \in L^2(\mathbb{R})$. Note that $(\mathcal{L} - z\mathrm{I})^{-1} : L^2(\mathbb{R}) \to H^n(\mathbb{R})$ is a well-defined bounded linear operator as long as $z \notin \mathrm{spec}(\mathcal{L})$, and we assume that $\mathcal{L}$ has no essential spectrum in the closed right half-plane. Then the homological equation has a unique solution in $H^n(\mathbb{R})$ as long as $z = m_1\lambda_1 + \cdots + m_M\lambda_M$ is not an eigenvalue of $DF(u_*)$. Observing that $\mathrm{real}(z) > 0$ we see that this reduces to the scalar nonresonance condition

$$m_1\lambda_1 + \cdots + m_M\lambda_M \neq \lambda_j \tag{28}$$

for $1 \leq j \leq M$. These are the finitely many nonresonance conditions which always appear in the parameterization method. They are the obstruction to the existence of a formal series conjugating the nonlinear dynamics to linear. See, again, [6, 7, 8].

The nonresonance conditions of (28) are valuable in practice as they are scalar conditions which warn us whether or not to proceed with the manifold calculation. Suppose, for example, that we compute the eigenvalues of $\mathcal{L}$ using the Evans function, and that we want to compute the polynomial approximation of the unstable manifold parameterization to order $N \in \mathbb{N}$. Then we simply check the nonresonance for each multi-index $(m_1, \dots, m_M) \in \mathbb{N}^N$ with $2 \leq m_1 + \cdots + m_M \leq N$. If there are no resonances to order N then we know in advance that we will be able to solve each of the homological equations defining the Taylor coefficients and we are confident committing the computational resources.

Assuming there are no resonances the homological equations uniquely determine the coefficients for all orders greater than or equal to two. This says that once the first order data are chosen, the parameterization P solving (4) is unique. But the only free choice in the first order data is the choice of the scalings of the eigenvectors. Put another way, the parameterization P is unique up to the choice of the eigenvector scaling. This nonuniqueness is exploited in numerical calculations where we use it to control the growth of the coefficients. Indeed, the scalings of the eigenvectors determine the decay rate of the norms $\|p_{m_1,\dots,m_M}\|_{H^n(\mathbb{R})}$ and can in general be chosen so that the growth condition of (25) is satisfied. In the present work we are not concerned with the convergence of the formal series and refer the interested reader to [26, 91] for convergence results in other contexts, though we do report the numerically observed convergence rates in some explicit examples below. Finally we remark that the entire discussion generalizes to systems of PDEs with only the obvious modifications, as illustrated in section 4.

3.2. Cauchy products of power series. Derivation of homological equations in the applications below relies on some formal power series manipulations. These calculations are much cleaner if we introduce a little notation. In particular, since our example systems are nonlinear, products of power series are a critical operation. In the present work we consider polynomial systems with only quadratic and cubic nonlinearities. We remark that higher degree polynomials are treated similarly. Moreover, using techniques from automatic differentiation for power series it is possible to transform nonpolynomial systems into polynomial systems of a larger number of variables. For explicit examples of this procedure for parabolic PDEs see [27]. A more abstract discussion is found in Chapter 2 of [24].

For the present work it is enough to consider the Cauchy product of two or three power series in one or two variables. Consider then the three power series of a single variable given

by

$$P(\theta) = \sum_{n=0}^{\infty} p_n \theta^n,$$

$$Q(\theta) = \sum_{n=0}^{\infty} q_n \theta^n,$$

and

$$R(\theta) = \sum_{n=0}^{\infty} r_n \theta^n.$$

The pointwise products of $P \cdot Q$ and $P \cdot Q \cdot R$ are expressed as power series via the Cauchy product formulas

$$(P \cdot Q)(\theta) = \sum_{n=0}^{\infty} (p * q)_n \theta^n,$$

and

$$(P \cdot Q \cdot R)(\theta) = \sum_{n=0}^{\infty} (p * q * r)_n \theta^n,$$

where

$$(p * q)_n = \sum_{j=0}^{n} p_{n-j} q_j$$

and

$$(p * q * r)_n = \sum_{j=0}^{n} \sum_{k=0}^{j} p_{n-j} q_{j-k} r_k.$$

Suppose we want to isolate the highest order terms from the Cauchy products. We have that

$$\begin{aligned}(p * q)_n &= \sum_{j=0}^{n} p_{n-j} q_j \\ &= p_0 q_n + q_0 p_n + \sum_{j=1}^{n-1} p_{n-j} q_j \\ &= p_0 q_n + q_0 p_n + (p \hat{*} q)_n,\end{aligned}$$

where we define

$$(p \hat{*} q)_n = \sum_{j=1}^{n-1} p_{n-j} q_j.$$

For the cubic term we have that

$$(p * q * r)_n = p_0 q_0 r_n + q_0 r_0 p_n + p_0 r_0 q_n + (p \hat{*} q \hat{*} r)_n,$$

where

$$(p\hat{*}q\hat{*}r)_n = \sum_{j=0}^{n}\sum_{k=0}^{j}\hat{\delta}_{njk}p_{n-j}q_{j-k}r_k,$$

where the term $\hat{\delta}_{njk}$ is defined by

$$\hat{\delta}_{jk}^{nj} = \begin{cases} 0 & \text{if } j=k=0, \\ 0 & \text{if } j=k=n, \\ 0 & \text{if } k=0 \text{ and } j=n, \\ 1 & \text{otherwise,} \end{cases}$$

and appears so that terms of order n are removed from the Cauchy product. The point is that the so called "hat products" do not depend on terms of order n.

Similarly, consider three power series of two variables:

$$P(\theta_1,\theta_2) = \sum_{n=0}^{\infty}\sum_{m=0}^{\infty}p_{mn}\theta_1^m\theta_2^n,$$

$$Q(\theta_1,\theta_2) = \sum_{n=0}^{\infty}\sum_{m=0}^{\infty}q_{mn}\theta_1^m\theta_2^n,$$

and

$$R(\theta_1,\theta_2) = \sum_{n=0}^{\infty}\sum_{m=0}^{\infty}r_{mn}\theta_1^m\theta_2^n.$$

Define the Cauchy products

$$(P\cdot Q)(\theta_1,\theta_2) = \sum_{n=0}^{\infty}\sum_{m=0}^{\infty}(p*q)_{mn}\theta_1^m\theta_2^n$$

and

$$(P\cdot Q\cdot R)(\theta_1,\theta_2) = \sum_{n=0}^{\infty}\sum_{m=0}^{\infty}(p*q*r)_{mn}\theta_1^m\theta_2^n,$$

where

$$(p*q)_{mn} = \sum_{i=0}^{m}\sum_{j=0}^{m}p_{m-i,n-j}q_{ij}$$

and

$$(p*q*r)_{mn} = \sum_{i=0}^{m}\sum_{j=0}^{i}\sum_{k=0}^{n}\sum_{l=0}^{k}p_{m-i,n-k}q_{i-j,k-l}r_{jl}.$$

In this case we have that

$$(p*q)_{mn} = p_{00}q_{mn} + q_{00}p_{mn} + (p\hat{*}q)_{mn}$$

and

$$(p * q * r)_{mn} = p_{00}q_{00}r_{mn} + p_{00}r_{00}q_{mn} + q_{00}r_{00}p_{mn} + (p\hat{*}q\hat{*}r)_{mn},$$

where

$$(p\hat{*}q)_{mn} = \sum_{i=0}^{m}\sum_{j=0}^{n} \hat{\delta}^{nj}_{mi} p_{m-i,n-j}q_{ij}$$

and

$$(p\hat{*}q\hat{*}r)_{mn} = \sum_{i=0}^{m}\sum_{j=0}^{i}\sum_{k=0}^{n}\sum_{l=0}^{k} \hat{\delta}^{nkl}_{mij} p_{m-i,n-k}q_{i-j,k-l}r_{jl}$$

with

$$\hat{\delta}^{nj}_{mi} = \begin{cases} 0 & \text{if } i = j = 0, \\ 0 & \text{if } i = m \text{ and } j = n, \\ 1 & \text{otherwise,} \end{cases}$$

and

$$\hat{\delta}^{nkl}_{mij} = \begin{cases} 0 & \text{if } i = k = 0, \\ 0 & \text{if } j = m \text{ and } l = n, \\ 0 & \text{if } i = m, k = n, j = 0, \text{ and } l = 0, \\ 1 & \text{otherwise.} \end{cases}$$

Remark 3.1 (formal calculation versus numerical implementations). It is worth noting that the formulas discussed above may not lead to the most efficient numerical implementations. For example it may be preferable to compute u^N by repeated Cauchy products, especially if the intermediate products $u^2, u^3, \ldots, u^{N-1}$ are also desired. Moreover, state-of-the-art polynomial manipulation libraries typically employ the fast Fourier transform algorithm for multiplying polynomials, especially in the multivariate case.

That being said, it should be noted that the hat products have

$$(p\hat{*}q\hat{*}r) \neq (p\hat{*}q)\hat{*}r \neq p\hat{*}(q\hat{*}r),$$

so that the formulas above should be kept in mind in formal series calculations. Optimal implementation of these products is not the topic of the present work.

3.3. Homological equations for Nagumo's equation. Since Nagumo's equation has one unstable eigenvalue λ, the unstable manifold is one dimensional and we look for $P(\theta, x)$ with $x \in \mathbb{R}$ and $\theta \in [-r, r]$ parameterizing the unstable manifold. The value of r is a priori unknown and is in fact set only after some numerical experimentation.

Assume that the parameterization has the power series expansion

$$P(\theta, x) = \sum_{n=0}^{\infty} p_n(x)\theta^n.$$

Imposing the first order conditions, $P(0, x) = p_0(x) = u_*(x)$ is the wave profile and $\frac{\partial}{\partial\theta}P(\theta, x)|_{\theta=0} = p_1(x) = \xi(x)$ is the eigenfunction.

The invariance equation (4) for a one dimensional unstable manifold reduces to

$$\lambda\theta\frac{\partial}{\partial\theta}P(\theta,x)=F(P(\theta,x)),$$

where for the Nagumo equation

$$F(P(\theta,x))=\frac{\partial^2}{\partial x^2}P(\theta,x)-P(\theta,x)+P(\theta,x)^3.$$

We describe the formal series calculation in some detail, for reasons which will become clear by the end.

Substituting the power series ansatz into the invariance equation we have

$$\begin{aligned}\lambda\theta\frac{\partial}{\partial\theta}P(\theta,x)&=\lambda\theta\frac{\partial}{\partial\theta}\left(\sum_{n=0}^{\infty}p_n(x)\theta^n\right)\\&=\lambda\theta\sum_{n=0}^{\infty}np_n(x)\theta^{n-1}\\&=\sum_{n=0}^{\infty}\lambda np_n(x)\theta^n\end{aligned}$$

on the left and

$$\begin{aligned}F(P(\theta,x))&=\frac{\partial^2}{\partial x^2}\left(\sum_{n=0}^{\infty}p_n(x)\theta^n\right)-\sum_{n=0}^{\infty}p_n(x)\theta^n+\left(\sum_{n=0}^{\infty}p_n(x)\theta^n\right)^3\\&=\sum_{n=0}^{\infty}p_n''(x)\theta^n-\sum_{n=0}^{\infty}p_n(x)\theta^n+\sum_{n=0}^{\infty}(p*p*p)_n(x)\theta^n\\&=\sum_{n=0}^{\infty}\left(p_n''(x)-p_n(x)+3p_0(x)^2p_n(x)+(p\hat{*}p\hat{*}p)_n(x)\right)\theta^n\end{aligned}$$

on the right. By matching like powers we obtain that

$$\lambda np_n(x)=p_n''(x)-p_n(x)+3p_0(x)^2p_n(x)+(p\hat{*}p\hat{*}p)_n(x),$$

and isolating terms of order n on the left leads to the homological equation

$$p_n''(x)+\left(-1+3p_0(x)^2\right)p_n(x)-\lambda np_n(x)=-(p\hat{*}p\hat{*}p)_n(x). \tag{29}$$

We require that $p_n(x)\to 0$ as $x\to\pm\infty$.

Observe that (29) does in fact have the form

$$[DF(p_0(x))-\lambda n\mathrm{Id}]\,p_n(x)=R_n(x)$$

with $R_n(x)$ given explicitly by

$$R_n(x)=-(p\hat{*}p\hat{*}p)_n(x),$$

just as claimed in section 3.1. The important point, in fact the entire reason for working through the formal calculation just given, is that we obtain explicitly the form of the right-hand side $R_n(x)$.

Introducing the variable $q_n(x) = p_n'(x)$ we write (29) as a first order system, giving rise to the boundary value problem,

$$\begin{pmatrix} p_n'(x) \\ q_n'(x) \end{pmatrix} = \begin{pmatrix} 0 & 1 \\ 1+\lambda n - 3p_0^2(x) & 0 \end{pmatrix} \begin{pmatrix} p_n(x) \\ q_n(x) \end{pmatrix} - \begin{pmatrix} 0 \\ \sum_{k=0}^{n} \sum_{r=0}^{k} \delta_{k,r}^{n} p_{n-k}(x) p_{k-r}(x) p_r(x) \end{pmatrix}. \tag{30}$$

We impose projective boundary conditions on (30) that select the solution that decays as $x \to \pm\infty$. That is, the solution to (30) that we approximate is tangent to the stable and unstable manifolds associated with the linear ODE system

$$\begin{pmatrix} p_n(x) \\ p_n'(x) \end{pmatrix}' = \begin{pmatrix} 0 & 1 \\ 1+\lambda n & 0 \end{pmatrix} \begin{pmatrix} p_n(x) \\ p_n'(x) \end{pmatrix} \tag{31}$$

at $x = \pm\infty$. Specifically, the boundary conditions are

$$P_L \cdot p_n(-L) = 0, \quad P_R \cdot p_n(L) = 0, \tag{32}$$

where $P_L = (-\sqrt{1+\lambda n}, 1)^T$ and $P_R = (\sqrt{1+\lambda}n, 1)^T$, and the truncated domain is $[-L, L]$.

To approximate well the solution $P_n(x) = (p_n(x), q_n(x))^T$ of (30) posed on the whole real line, we must choose L sufficiently large. In practice, we take L large enough that $|p_n(\pm L)| < 10^{-8}$. For Nagumo's equation, $L = 20$ satisfies this choice.

To speed up the computation, we use Chebyshev polynomial interpolation of the numerical approximations of the solutions $p_n(\cdot)$ of the homological equations, which greatly speeds up the evaluation of the farthest right term in (30) when using the MATLAB routine *bvp5c*. It is faster to evaluate a Chebyshev polynomial interpolant then to use the routine *deval* built into MATLAB. Increasing L requires higher degree Chebyshev polynomial interpolants.

3.4. Gray–Scott's homological equations. Recall that the Gray–Scott equations have the unstable eigenvalue $\lambda \approx 8.6267$, and take the profiles u_*, v_* and eigenfunctions as discussed in section 2.3.2. Since the unstable manifold is one dimensional we make the power series ansatz

$$\vec{P}(\theta, x) = \begin{bmatrix} P(\theta, x) \\ Q(\theta, x) \end{bmatrix} = \sum_{n=0}^{\infty} \begin{bmatrix} u_n(x) \\ v_n(x) \end{bmatrix} \theta^n = \sum_{n=0}^{\infty} \vec{p}_n(x) \theta^n, \tag{33}$$

where $u_0(x) = u_*(x)$, $v_0(x) = v_*(x)$, $u_1(x) = \xi(x)$, and $v_1(x) = \eta(x)$.

In this case the invariance equation reduces to

$$\lambda\theta \frac{\partial}{\partial\theta} \vec{P}(\theta, x) = F(\vec{P}(\theta, x)),$$

where, as before,

$$\lambda\theta \frac{\partial}{\partial\theta} \vec{P}(\theta, x) = \sum_{n=0}^{\infty} n\lambda \vec{p}_n(x) \theta^n$$

and

$$F(\vec{P}(\theta,x)) = \begin{pmatrix} \frac{\partial^2}{\partial x^2}P(\theta,x) - P(\theta,x)Q(\theta,x)^2 + \alpha(1-P(\theta,x)) \\ \frac{\partial^2}{\partial x^2}Q(\theta,x) - \frac{1}{\gamma}Q(\theta,x) + \frac{1}{\gamma}P(\theta,x)Q(\theta,x)^2 \end{pmatrix}.$$

A calculation following the same steps as in section 3.3 shows that for $n \geq 2$ the coefficients $\vec{p}_n(x)$ must satisfy,

$$\begin{aligned} u_n''(x) - (\alpha + n\lambda)u_n(x) - v_*(x)^2 u_n(x) - 2u_* v_* v_n(x) &= (u\hat{*}v\hat{*}v)_n, \\ v_n''(x) - n\lambda v_n(x) + \frac{1}{\gamma}\left(v_*(x)^2 u_n(x) + 2u_* v_* v_n(x) - v_n(x)\right) &= -\frac{1}{\gamma}(u\hat{*}v\hat{*}v)_n \end{aligned} \tag{34}$$

which again has the desired form

$$(DF(u_*, v_*) - n\lambda \mathrm{Id})\,\vec{p}_n(x) = R_n(x),$$

and recovers the explicit form of $R_n(x)$.

Introducing the variables $p_n(x) = u_n'(x)$ and $q_n(x) = v_n'(x)$, the homological equations can be rewritten as a first order system, giving rise to the BVP

$$\begin{pmatrix} u_n'(x) \\ p_n'(x) \\ v_n'(x) \\ q_n'(x) \end{pmatrix} = \begin{pmatrix} 0 & 1 & 0 & 0 \\ \alpha + n\lambda + v_*^2 & 0 & u_* v_* & 0 \\ 0 & 0 & 0 & 1 \\ -\frac{v_*^2}{\gamma} & 0 & \frac{1}{\gamma} + n\lambda - \frac{2}{\gamma}u_* v_* & 0 \end{pmatrix} \begin{pmatrix} u_n \\ p_n \\ v_n \\ q_n \end{pmatrix} + \begin{pmatrix} 0 \\ b_n \\ 0 \\ -\frac{1}{\gamma}b_n \end{pmatrix}, \tag{35}$$

where $b_n := (u\hat{*}v\hat{*}v)_n$.

Let

$$A_n = \begin{pmatrix} 0 & 1 & 0 & 0 \\ \alpha - n\lambda & 0 & 0 & 0 \\ 0 & 0 & 0 & 1 \\ 0 & 0 & n\lambda & 0 \end{pmatrix}$$

and $W_n(x) = (u_n(x), p_n(x), v_n(x), q_n(x))^T$. Define P_n^1, P_n^2 and P_n^3, P_n^4 to be the unstable and the stable eigenvectors of A_n, respectively, and let $\mathbb{E}_n^+ = \mathrm{span}(P_n^1, P_n^2)$ and $\mathbb{E}_n^- = \mathrm{span}(P_n^3, P_n^4)$. We choose $L = 25$ so that $|P_n(\pm L)| < 10^{-8}$, and impose the projected boundary condition $W_n(-L) \in \mathbb{E}_+$ and $W_n(L) \in \mathbb{E}_+$ to numerically solve the homological equation.

3.5. Schrödinger's homological equations. Suppose that $u_*(x), v_*(x)$ is an equilibrium (standing wave) solution of the Schrödinger equation with complex conjugate eigenvalues

$$\lambda_{1,2} = \alpha \pm i\beta,$$

and that the corresponding complex conjugate eigenvectors $\xi(x) = (\xi_1(x), \xi_2(x))$, and $\eta(x) = (\eta_1(x), \eta_2(x))$ satisfy

$$\overline{\xi(x)} = \eta(x).$$

Let

$$P(\theta_1, \theta_2, x) = \sum_{m=0}^{\infty}\sum_{n=0}^{\infty} \begin{bmatrix} u_{mn}(x) \\ v_{mn}(x) \end{bmatrix} \theta_1^m \theta_2^n$$

with

$$u_{00}(x) = u_0(x), \qquad v_{00} = v_0(x),$$

and where

$$u_{10}(x) = \xi_1(x), \qquad v_{10} = \xi_2(x), \qquad u_{01}(x) = \eta_1(x), \qquad v_{01} = \eta_2(x),$$

are the components of the eigenfunction. Since the unstable manifold is two dimensional the invariance equation in this case reduces to

$$\lambda_1\theta_1\frac{\partial}{\partial\theta_1}P(\theta_1,\theta_2,x) + \lambda_2\theta_2\frac{\partial}{\partial\theta_2}P(\theta_1,\theta_2,x) = F(P(\theta_1,\theta_2,x)).$$

Substituting in the power series ansatz leads to

$$\lambda_1\theta_1\frac{\partial}{\partial\theta_1}P(\theta_1,\theta_2,x) + \lambda_2\theta_2\frac{\partial}{\partial\theta_2}P(\theta_1,\theta_2,x) = \sum_{m=0}^{\infty}\sum_{n=0}^{\infty}(\lambda_1 m + \lambda_2 n)\begin{bmatrix} u_{mn}(x) \\ v_{mn}(x)\end{bmatrix}\theta_1^m\theta_2^n,$$

on the left and

$$F(P(\theta_1,\theta_2,x))$$
$$= \sum_{m=0}^{\infty}\sum_{n=0}^{\infty}\begin{pmatrix} -v''_{mn}(x) + \mu v_{mn}(x) - (v*v*v)_{mn} - (v*u*u)_{mn} \\ u''_{mn}(x) - u_{mn}(x) + (u*v*v)_{mn} + (u*u*u)_{mn} - 2\nu v_{mn}\end{pmatrix}\theta_1^m\theta_2^n,$$

on the right. Matching like powers leads to

$$(\lambda_1 m + \lambda_2 n)\begin{pmatrix} u_{mn} \\ v_{mn}\end{pmatrix}$$
$$= \begin{pmatrix} -v''_{mn}(x) + \mu v_{mn}(x) - (v*v*v)_{mn} - (v*u*u)_{mn} \\ u''_{mn}(x) - u_{mn}(x) + (u*v*v)_{mn} + (u*u*u)_{mn} - 2\nu v_{mn}\end{pmatrix}$$
$$= \begin{pmatrix} -v''_{mn} + \mu v_{mn} - 3v_*^2 v_{mn} - (v\hat{*}v\hat{*}v)_{mn} - u_*^2 v_{mn} - 2v_* u_* u_{mn} - (v\hat{*}u\hat{*}u)_{mn} \\ u''_{mn} - u_{mn} + 2u_* v_* v_{mn} + v_*^2 u_{mn} + (u\hat{*}v\hat{*}v)_{mn} + 3u_*^2 u_{mn} + (u\hat{*}u\hat{*}u)_{mn} - 2\nu v_{mn}\end{pmatrix}.$$

Observe that (after choosing an appropriate norm) the Fréchet derivative of F at (u_*, v_*) acting on $(u,v)^T$ is

$$DF(u_*,v_*)\begin{bmatrix} u \\ v\end{bmatrix} = \begin{bmatrix} -v'' + \mu v - 3v_*^2 v - 2u_* v_* u - u_*^2 v \\ u'' - u + 2u_* v_* v + v_*^2 u + 3u_*^2 u - 2\nu v\end{bmatrix}$$

so that the homological equations indeed have the form

$$(DF(u_0,v_0) - (m\lambda_1 + n\lambda_2)\mathrm{Id})\begin{bmatrix} u_{mn} \\ v_{mn}\end{bmatrix} = R_{mn}(x),$$

just as they must. We stress once again that the entire point of going through the formal series calculations above is that we obtain explicitly the expression

$$R_{mn}(x) = \begin{bmatrix} -(u\hat{*}u\hat{*}u)_{mn} - (u\hat{*}v\hat{*}v)_{mn} \\ (v\hat{*}u\hat{*}u)_{mn} - (v\hat{*}v\hat{*}v)_{mn}\end{bmatrix}$$

for the right-hand side. The fact that the left-hand side comes out correctly provides a convenient check on our work.

Introducing the variables $p_{mn} = u'_{mn}$ and $q_{mn} = v'_{mn}$ and defining the matrices

$$A_{mn}(x) = \begin{pmatrix} 0 & 1 & 0 & 0 \\ 1 - 3u_*(x)^2 - v_*(x)^2 & 0 & (\lambda_1 n + \lambda_2 m) + 2\nu - 2u_*(x)v_*(x) & 0 \\ 0 & 0 & 0 & 1 \\ -(\lambda_1 n + \lambda_m) - 2u_*(x)v_*(x) & 0 & \mu - 3v_*(x)^2 - u_*(x)^2 & 0 \end{pmatrix}$$

we rewrite the homological equations as the linear system

$$\begin{pmatrix} u'_{nm} \\ p'_{nm} \\ v'_{nm} \\ q'_{nm} \end{pmatrix} = A_{mn} \begin{pmatrix} u_{nm} \\ p_{nm} \\ v_{nm} \\ q_{nm} \end{pmatrix} - \begin{pmatrix} 0 \\ N^1_{mn} \\ 0 \\ N^2_{mn} \end{pmatrix}, \tag{36}$$

where

$$N^1_{mn} := (u \hat{*} u \hat{*} u)_{mn} + (u \hat{*} v \hat{*} v)_{mn},$$
$$N^2_{mn} := (v \hat{*} u \hat{*} u)_{mn} + (v \hat{*} v \hat{*} v)_{mn}.$$

The limiting matrix for the linear portion of (36) is given by

$$A_{mn} = \begin{pmatrix} 0 & 1 & 0 & 0 \\ 1 & 0 & (\lambda_1 n + \lambda_2 m) + 2\nu & 0 \\ 0 & 0 & 0 & 1 \\ -(\lambda_1 n + \lambda_2 m) & 0 & \mu & 0 \end{pmatrix}. \tag{37}$$

Let $W_{mn}(x) = (u_{mn}(x), p_{mn}(x), v_{mn}(x), q_{mn}(x))^T$ and define $P^1_{m,n}, P^2_{m,n}$ and $P^3_{m,n}, P^4_{m,n}$ to be the unstable and the stable eigenvectors of $A_{m,n}$, respectively, and let $\mathbb{E}_+ = \text{span}(P^1_{m,n}, P^2_{m,n})$ and $\mathbb{E}_- = \text{span}(P^3_{m,n}, P^4_{m,n})$. We choose $L = 300$ which ensures that $|P_n(\pm L)| < 10^{-8}$, and impose the projected boundary condition $W_{m,n}(-L) \in \mathbb{E}_+$ and $W_{m,n}(L) \in \mathbb{E}_+$ to numerically solve the homological equation.

4. Numerical implementation and example calculations. Consider again the parabolic PDE

$$u_t = \mathcal{F}(u),$$

as discussed in section 3.1. In all of the examples considered in the present work, $\mathcal{F}$ is densely defined on a Hilbert space $\mathcal{H}$. The numerical procedure for computing the unstable manifold parameterization is as follows.

- *Step* 1: Numerically solve the profile equation $\mathcal{F}(u) = 0$ to find a traveling wave $u_* \in \mathcal{H}$. Let $p_0 = u_*$.
- *Step* 2: Suppose that the standing wave is unstable with Morse index M. If $M = 0$ the wave is stable and the unstable manifold is empty. In this case we end the procedure. Otherwise numerically solve the eigenvector problem

$$D\mathcal{F}(p_*)\xi = \lambda\xi$$

to find the unstable eigenvalues $\lambda_1, \dots, \lambda_M$ and associated eigenfunctions $\xi_1, \dots, \xi_M \in \mathcal{H}$. Set $p_{e_j} = \xi_j$, where e_j is the vector with a 1 in the jth component and zeros elsewhere.

- *Step* 3: Check the nonresonance conditions

$$m_1\lambda_1 + \cdots + m_M\lambda_M \neq \lambda_j,$$

$(m_1, \dots, m_M) \in \mathbb{N}^M$ with $m_1 + \cdots + m_M \geq 2$ and for each $1 \leq j \leq M$. (This is actually only a finite number of conditions as the λ_j are all unstable). If there is a resonance at order $\tilde{N} \geq 2$ choose $N < \tilde{N}$. If there are no resonances then we are free to approximate the parameterization to any desired order $N \geq 2$.

- *Step* 4: For all $(m_1, \dots, m_M) \in \mathbb{N}^M$ with $m_1 + \cdots + m_M \geq 2$ solve the homological equation

$$[D\mathcal{F}(p_*) - (m_1\lambda_1 + \cdots + m_M\lambda_M)\mathrm{Id}]\, p_{m_1,\dots,m_M} = -R_{m_1,\dots,m_M},$$

where $p_{m_1,\dots,m_M} \in \mathcal{H}$. This is a projected boundary value problem on the line. The equation has a unique solution as there are no resonances up to order N. Return the power series coefficients $p_{m_1,\dots,m_M}$ for $0 \leq m_1 + \cdots + m_M \leq N$.

We refer to this as *the main algorithm*. The polynomial

$$P^N(x, \theta_1, \dots, \theta_M) = \sum_{0 \leq m_1 + \cdots + m_M \leq N} p_{m_1,\dots,m_M}(x)\theta_1^{m_1} \dots \theta_M^{m_M},$$

approximates the unstable manifold to order N.

As a postprocessing step we check the a posteriori error associated with P^N as follows. Choose an allowed error tolerance $\varepsilon \ll 1$ and for some large $K \in \mathbb{N}$ choose some sample points $\{\vec{\theta}_k\}_{k=1}^K \in \mathbb{B}$ throughout the domain of P^N. For some $\tau > 0$ and for each $1 \leq k \leq K$ define $\widetilde{\vec{\theta}}_k$ by

$$\widetilde{\vec{\theta}}_k = e^{-\Lambda_M \tau}\vec{\theta}_k.$$

Here

$$\Lambda_M = \begin{pmatrix} \lambda_1 & \dots & 0 \\ \vdots & \ddots & \vdots \\ 0 & \dots & \lambda_M \end{pmatrix}$$

is the diagonal matrix of eigenvalues. Compute the quantities

$$\epsilon_k = \|\Phi_{\mathrm{num}}(\widetilde{\vec{\theta}}_k, \tau) - P(\vec{\theta}_k)\|_{\mathcal{H}},$$

where Φ_{num} is a numerical integration scheme for the parabolic PDE. We are satisfied with the calculation if

$$\max(\epsilon_1, \dots, \epsilon_K) \leq \varepsilon.$$

If the check fails then we can decrease the size of the box $\mathbb{B} = [-r_1, r_1] \times \cdots \times [-r_M, r_M]$ (or decrease the scalings of the eigenfunctions) and rerun the main algorithm. On the other

hand it may turn out that the $\epsilon_1, \ldots, \epsilon_K$ are all dramatically less than ε. In this case we can increase the size of the domain (or the scalings of the eigenvectors) and run the main algorithm again.

Automatic procedures for choosing optimal scalings for the eigenvectors are discussed in [91]. In the present work we employ the heuristic that the Nth order coefficients should be on the order of the absolute error tolerance of the BVP solver used to solve the homological equations, or smaller. This is usually enough to guarantee that $\max(\epsilon_1, \ldots, \epsilon_K)$ is less than ε. We note that we can approximate how large we may take $\vec{\theta_K}$ via the heuristic we now describe. Suppose the parameterization is given by

$$P(\theta_1, \ldots, \theta_M, x) = \sum_{m_1=0}^{\infty} \cdots \sum_{m_M=0}^{\infty} p_{m_1,\ldots,m_M}(x) \theta_1^{m_1} \ldots \theta_M^{m_M},$$

and that $\tilde{p}_{m_1,\ldots,m_M}(x)$ (may be zero) is our numerical approximation of $p_{m_1,\ldots,m_M}(x)$ for each pair of indices. Further suppose that $\max_{m_1,\ldots,m_M,x} |p_{m_1,\ldots,m_M}(x) - \tilde{p}_{m_1,\ldots,m_M}(x)| < \zeta$ for some $\zeta > 0$ and each pair of indices. The tolerance for the BVP solver is a good approximation of ζ. We note that,

$$\begin{aligned} P(\theta_1, \ldots, \theta_M, x) = & \sum_{m_1=0}^{\infty} \cdots \sum_{m_M=0}^{\infty} \tilde{p}_{m_1,\ldots,m_M}(x) \theta_1^{m_1} \ldots \theta_M^{m_M} \\ & + \sum_{m_1=0}^{\infty} \cdots \sum_{m_M=0}^{\infty} \left(p_{m_1,\ldots,m_M}(x) - \tilde{p}_{m_1,\ldots,m_M}(x)\right) \theta_1^{m_1} \ldots \theta_M^{m_M}. \end{aligned}$$

Thus the error of the numerical solution is bounded by

$$\sum_{m_1=0}^{\infty} \cdots \sum_{m_M=0}^{\infty} \left|\left(p_{m_1,\ldots,m_M}(x) - \tilde{p}_{m_1,\ldots,m_M}(x)\right) \theta_1^{m_1} \ldots \theta_M^{m_M}\right| \leq \zeta \sum_{m_1=0}^{\infty} \cdots \sum_{m_M=0}^{\infty} \left|\theta_1^{m_1} \ldots \theta_M^{m_M}\right|.$$

If we want the error of the parameterization method to be bounded by $\zeta_1 > \zeta$, then we take $\vec{\theta_K}$ such that $|\theta_1^{K_1}, \ldots, \theta_M^{K_M}| \leq \frac{\zeta_1}{\zeta}$.

We refer to the entire error checking procedure just described as *a posteriori verification* for the main algorithm.

4.1. Unstable manifold for Nagumo's equations. We use (30) in the main algorithm to recursively solve the first $N = 30$ homological equations. The first four generated solutions of the homological equations we denote by p_2, p_3, p_4, and p_5 and they are illustrated in Figure 8. These are the Taylor coefficients of the parameterization to order 5. Observe that the 5th order coefficients already have C^0 norm on the order of 10^{-5}. The maximum absolute value of the final homological equation solution ($N = 30$) is given by 6.290e-21. We choose a domain of $\mathbb{B} = [-2, 2]$ for the parameterization, that is, we take $r = 2$.

Figure 9 illustrates what the nonlinear unstable manifold looks like away from the stationary solution.

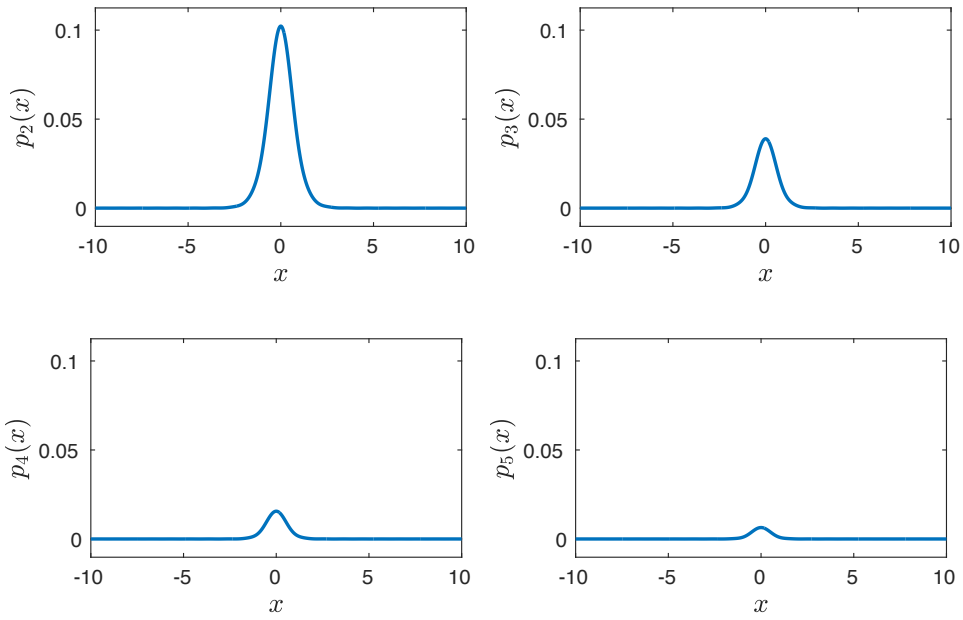

Figure 8. *Solutions to the first four generated homological equations, p_2, p_3, p_4, and p_5 for the Nagumo equation.*

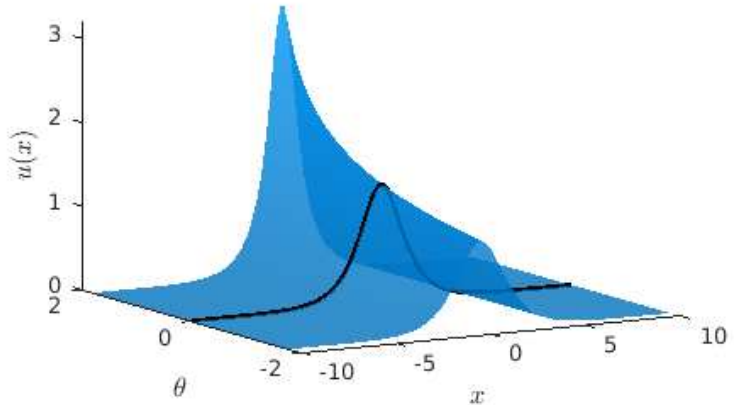

Figure 9. *Plot of $u(x)$ on the unstable manifold for Nagumo's equation with values of $\theta \in [-2, 2]$. The black line represents the profile/equilibrium solution.*

4.1.1. Finite difference verification of Nagumo. To verify the correctness of our approximation of the unstable manifold via the parameterization method, we employ the a posteriori verification scheme. For all systems in this work, we use the package provided in [28] to automatically produce finite difference code for the Crank–Nicolson method, giving the numerical integration scheme Φ_{num}. Recall that the Crank–Nicolson scheme is second order accurate for

Table 1

Convergence study results for Nagumo's equation. Here Δx in the distance between spatial grid points, and "Time" is how long the code ran for the associated value of Δx. The distance between temporal nodes is given by $\Delta t = \Delta x^2/4$. The last column shows the difference in the C^0 norm of the solutions of the time evolution and the parameterization method at the final time.

Δx	Time	$\|u_n - u_0\|_\infty$
2^{-2}	3.64e-1	6.53e-1
2^{-3}	1.45	9.36e2
2^{-4}	1.04e1	2.15e-2
2^{-5}	6.36e1	5.27e-3
2^{-6}	6.48e22	1.33e-3
2^{-7}	6.94e3	3.53e-4

the heat equation. Thus, we have cause to hope that the Crank–Nicolson scheme will also be second order accurate for the systems we consider. We will consider the parameterized nonlinear manifold to be verified correct if we initialize the finite difference time evolution code with a solution of the parameterization method and then observe convergence of order two of the finite difference scheme solution to the solution predicted by the parameterization after the same amount of time has passed. We remark that the accuracy and speed of the parameterization method compared to the finite difference scheme is one of the benefits of the former. Indeed, the limiting factor in the precision with which we verify the parameterization method is the computation time as the finite difference grid size decreases.

For verification of the main algorithm, we initialize the PDE with data corresponding to $\hat{\theta}_0 = 1/2$, and then we evolve forward in time by $T = 0.334$. The time elapsed between the two parameterization values $\hat{\theta}_0 = 1/2$ and $\hat{\theta}_1 = 1.36$ can be calculated as $\Delta T = (\log(\hat{\theta}_1) - \log(\hat{\theta}_0))/\lambda$. We begin the finite difference code at $u_0(x) = P^N(\hat{\theta}_0, x)$ and evolve it ΔT forward in time, denoting its final result as $u_n(x)$. Let $u_1(x) = P^N(\hat{\theta}_1, x)$. We then check that $\|u_n(x) - u_1(x)\|_{\text{inf}}$ is small and converges toward zero as the finite difference mesh becomes finer, which verifies the conjugacy condition holds, in turn verifying the code to solve the homological equations was correctly implemented. We performed a convergence study to check the conjugacy for $\Delta x = 2^{-k}$, $k \in \{2, \ldots, 7\}$, with $\frac{\Delta t}{\Delta x^2} = 0.25$. For the time evolution, we use Dirichlet boundary conditions matching the solution given by the parameterization method. Recall that we use projective boundary conditions to solve the homological equations. We truncate the domain to $[-L, L]$ where $L = 25$, which is large enough that the solutions to the homological equations evaluated on the boundary of the domain are within approximately 1e-8 of their asymptotic end states. We conclude that the method gives accurate results as seen by the rate of convergence shown in Table 1.

4.2. Unstable manifold for Gray–Scott. We use (35) combined with the main algorithm to recursively solve the first thirty homological equations. Several solutions of the homological equations are shown in Figure 10, a visualization of the manifold is pictured in Figure 11. In solving the homological equations, we take $L = 10$. We compute the parameterization to order $N = 25$ and find that the pointwise norm (Euclidean norm) over the coefficients of order $N = 25$ is smaller than $1.464e - 26$. We choose $r = 10$ so that $\mathbb{B} = [-10, 10]$ is the domain of the parameterization.

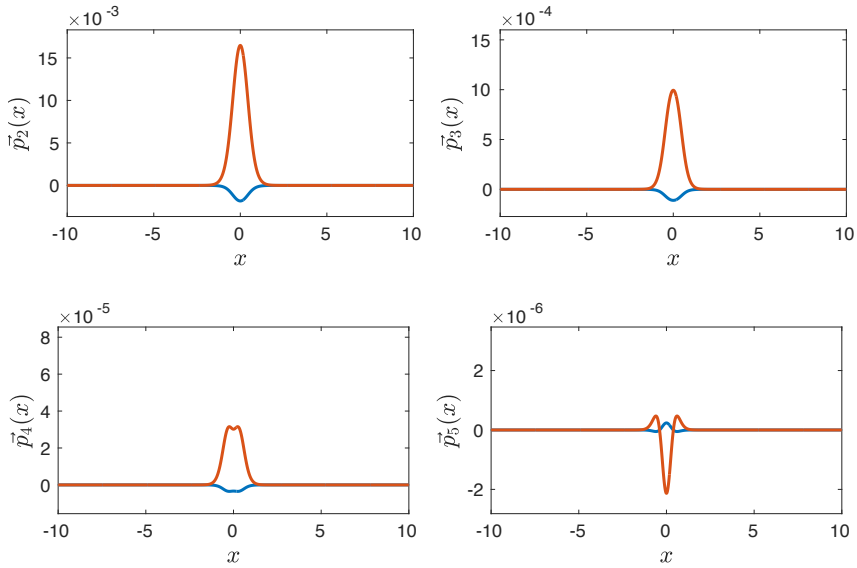

Figure 10. *The first four generated homological equations for the Gray–Scott equation. Note the scaling decreases in each consecutive figure.*

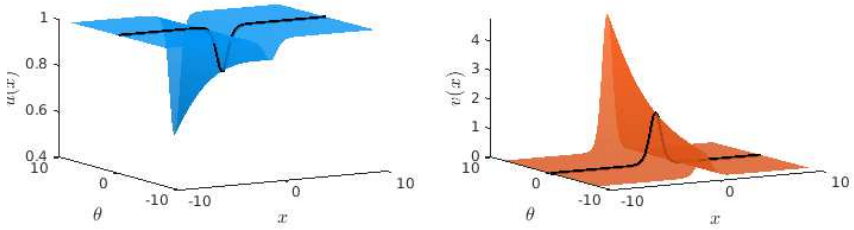

Figure 11. *Plot of $u(x)$ and $v(x)$ on the unstable manifold for the Gray–Scott system. Values of $\theta \in [-10, 10]$. The black line represents the profile/equilibrium solution. The u component is in the left frame (blue) while the v component is on the right (red).*

4.2.1. Finite difference verification of Gray–Scott. for the main algorithm. Evaluating our parameterization we obtain two solutions, U_0 and U_1, corresponding to values produced by the manifold at $\theta_0 = 0.1$ and $\theta_1 = 1.36$, respectively. For our initial state of the finite difference code, we choose U_0. We let $\Delta T = 0.303$ be the total time elapsed by our finite difference method and perform a convergence study by taking $\Delta x = 2^{-k}$ with $k \in \{2, \ldots, 8\}$ and $\frac{\Delta t}{\Delta x^2} = 0.25$. We truncate the domain to $[-L, L]$, where $L = 8$, which suffices to guarantee that the homological solutions evaluated on the boundaries are within approximately 1e-8 of their asymptotic end states. We use $N = 30$ homological equations in the computation. Table 2 shows the results.

4.3. Unstable manifold for Schrödinger's equation. We use (36) combined with the main algorithm to solve the first 20 homological equations. That is we compute the parameterization to order $N = 20$. The real and imaginary parts of several of the solutions to the homological equations are shown in Figure 12. To plot the unstable manifold, we require that $\theta_1 = \bar{\theta}_2$ and

Table 2

Convergence study results for Gray–Scott. Here Δx is the distance between spatial nodes of the mesh and "Time" is how long in seconds the finite difference code took to run. The distance between temporal nodes is given by $\Delta t = \Delta x^2/4$. The last column shows the distance between the solutions of the time evolution and the parameterization method at the final time $T = 0.303$, when initialized the same at $T = 0$ in the C^0 norm.

Δx	Time	$\|u_n - u_1\|_\infty$
2^{-2}	4.93e-1	2.54
2^{-3}	1.67	5.77e-1
2^{-4}	9.59	1.34e-1
2^{-5}	5.94e1	3.27e-2
2^{-6}	4.52e2	8.14e-3
2^{-7}	4.50e3	2.03e-3
2^{-8}	5.56e4	5.09e-4

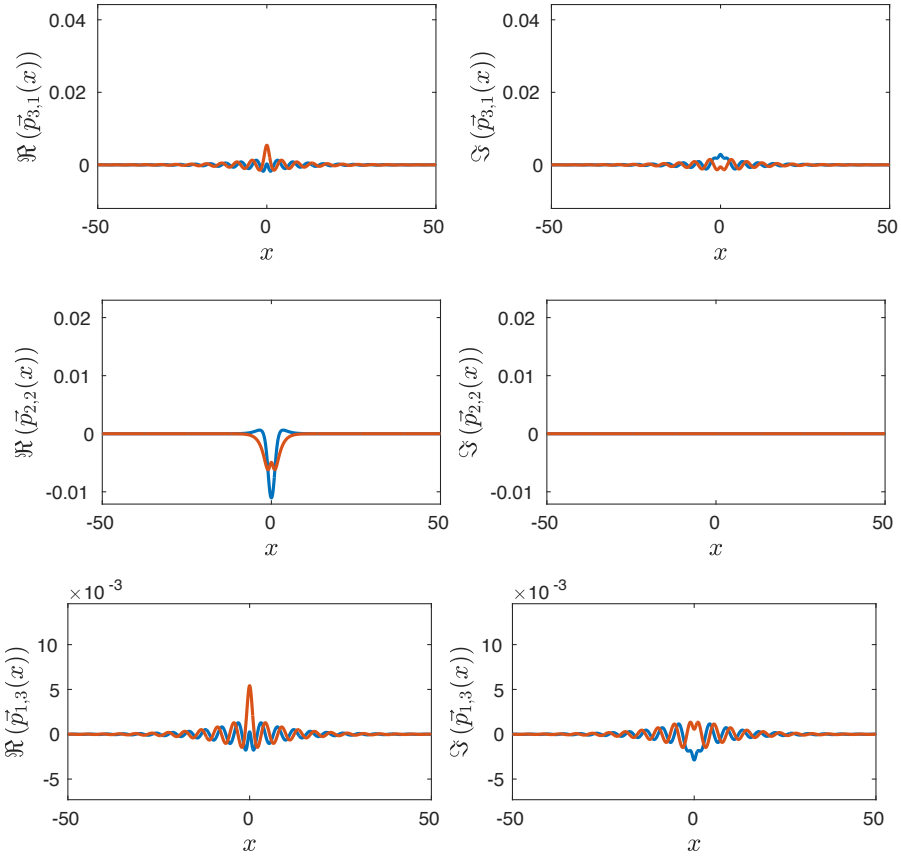

Figure 12. *The real and imaginary part of the first four generated homological equations for Schrödinger's equation. Note the scale gets smaller with each subsequent image.*

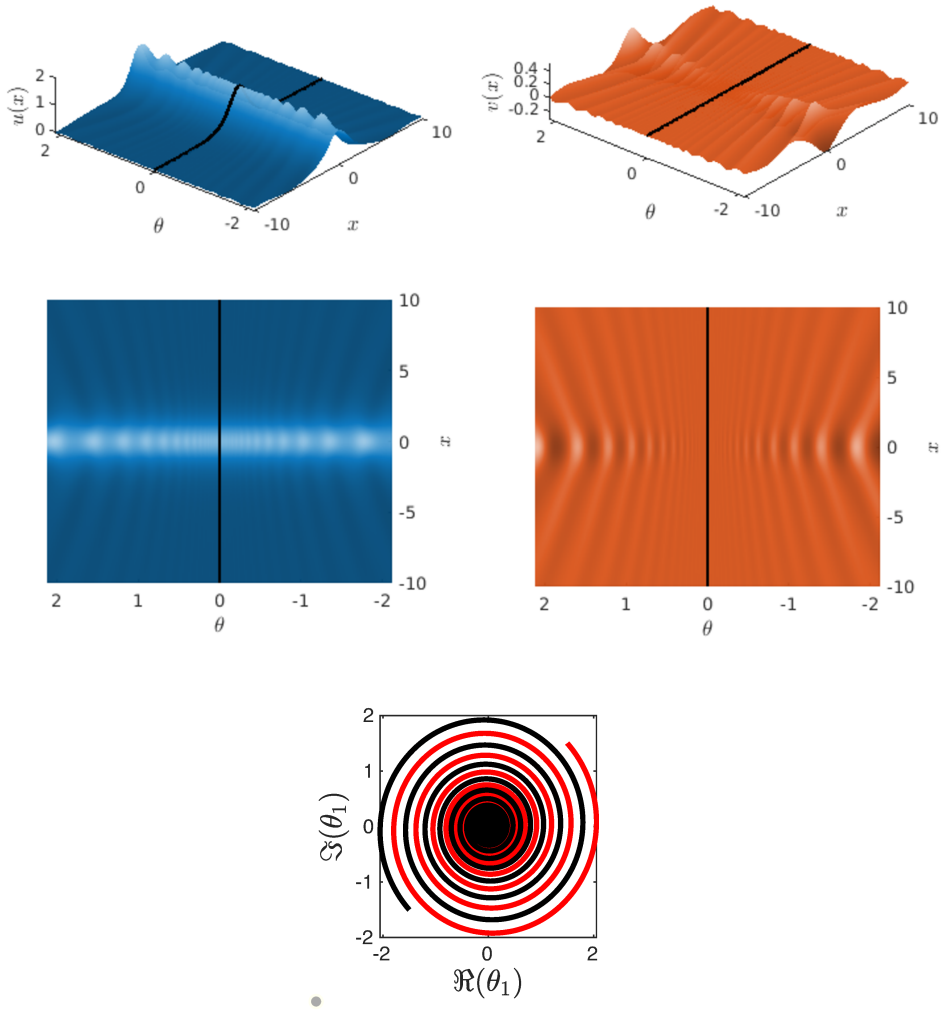

Figure 13. *The nonlinear manifold for the Schrödinger equation. Top left and right—$u(x)$ (blue) and $v(x)$ components of a solution on the unstable manifold of the equilibrium. The figure illustrates the oscillation of solutions as they converge (in backward time) to the equilibrium. Center left and right—same as above but a top-down view. Bottom—the corresponding orbit in parameter space. Recall that we are just past a Hopf bifurcation so that the real part of the complex conjugate eigenvalues is fairly small, approximately* 0.056. *This explains the spiraling in linear dynamics, and accounts for the fairly dramatic oscillation in the solutions on the unstable manifold.*

we vary θ_1 in an outward spiral in the complex plane as shown at the bottom of Figure 13. We also plot the manifold along the image of this spiral reflected across the imaginary axis. In Figure 13, $\theta = |\theta_1|$ along the black spiral, and $\theta = -|\theta_1|$ along the red spiral. Observe that, since the real part of the unstable eigenvalue is positive but small, the linear dynamics is fairly slow. This leads to a substantial oscillation on the manifold. In this case we take

Table 3

Convergence study results for Schrödinger's. Here Δx is the distance between spatial nodes of the mesh and "Time" is how long in seconds the finite difference code took to run. The distance between temporal nodes is given by $\Delta t = \Delta x^2/4$. The last column shows the distance between the solutions of the time evolution and the parameterization method at the final time $T = 1$, when initialized the same at $T = 0$ in the C^0 norm.

Δx	Time	$\|u_n - u_1\|_\infty$
2^{-2}	8.41	1.45e-2
2^{-3}	3.68	3.193-3
2^{-4}	1.86e2	8.74e-4
2^{-5}	9.57e2	5.55e-4

$r = 2$ and because we use complex conjugate variables the domain can be thought of as the disk with radius r.

4.3.1. Finite difference verification of Schrödinger's equation. We apply the a posteriori verification for the main algorithm. We follow the same process as outlined in section 4.1.1 to perform a convergence study. For the verification of the main algorithm, we take $L = 30$, $\frac{\Delta t}{\Delta x^2} = 1/4$, $\Delta T = 1$, and $\theta_1 = 1.5 + 1.5i$. We use 20 homological equations. Table 3 shows the results. To successfully solve the homological equations for Schrödinger's equation, we were only able to request an error tolerance of 1e-6 from the BVP solver, which explains the decreasing rate of convergence at the end of the table.

4.4. An application to traveling waves with nonzero wave speed. Although the examples considered up until now have been standing waves, we can apply the same method to traveling waves. We use Nagumo's equation with an additional transport term to illustrate the ideas in a fixed example. The treatment of general traveling waves follows similarly. To begin, consider the system

$$\tilde{u}_{\tilde{t}} = \tilde{u}_{\tilde{x}\tilde{x}} - \tilde{u}_{\tilde{x}} - \tilde{u} + \tilde{u}^3, \tag{38}$$

where $\tilde{u}(\tilde{x}, \tilde{t}) : \mathbb{R} \times (0, \infty) \to \mathbb{R}$. A traveling wave solution of (38) is given by

$$u_*(\tilde{x}) = \sqrt{2}\ \mathrm{sech}(\tilde{x} - \tilde{t}).$$

Under the coordinate change $x = \tilde{x} - \tilde{t}$, $t = \tilde{t}$, (38) becomes

$$u_t = u_{xx} - u + u^3,$$

which we recognize as Nagumo's equation given in (13). Thus, all of the computations described in section 4.1 apply to this system in the new coordinates. If $u(x, t)$ is the unstable manifold solution of (13) corresponding to the stationary wave $u^*(x) = \sqrt{2}\ \mathrm{sech}(x)$, then we find upon reversing the coordinate change that $\tilde{u}(\tilde{x}, \tilde{t}) := u(\tilde{x} - \tilde{t}, \tilde{t})$ is the unstable manifold solution to (38) corresponding to the unstable traveling wave solution $u_*(\tilde{x})$. Conceptually, the nonlinear manifold solution of (38) is the nonlinear manifold solution of (13) "moving along" at the speed of the traveling wave.

More generally, if $u_*(\tilde{x}, \tilde{t})$ is a traveling wave solution of the parabolic PDE

$$\tilde{u}_{\tilde{t}} = N(\tilde{u})$$

with constant speed c, where N is a partial differential operator, then by making the coordinate change $x = \tilde{x} - c\tilde{t}$, $t = \tilde{t}$, we obtain the PDE

$$u_t - cu_x = N(u), \tag{39}$$

which has $u^*(x) := u_*(x, 0)$ as a stationary wave solution. We may then carry out all of the methods of this paper to approximate the unstable manifold defined by $u(x, t)$ for the PDE given in (39), and then reverse the coordinate change to find the unstable manifold in the original coordinates, given by $\tilde{u}(\tilde{x}, \tilde{t}) := u(\tilde{x} - c\tilde{t}, \tilde{t})$.

5. Conclusions. In this paper we have presented a method for high order numerical approximation of unstable manifolds attached to traveling wave solutions for parabolic PDEs on the line. The unstable manifolds describe the time behavior of solutions which diverge from a small neighborhood of the unstable nonlinear wave. We developed a parameterization method which applies to nonlinear wave solutions and showed that the invariance equation can be solved using formal series methods. We derived the recursion relations, or homological equations, for the formal series solution in a number of example problems and showed that the homological equations are nonautonomous systems of linear equations on the line satisfying asymptotic boundary conditions. We implemented numerical methods for solving the homological equations in a number of interesting examples coming from applied mathematics. Using techniques of numerical integration for solving initial value problems for parabolic PDEs on the line we showed that our approximate manifolds provide a good description of the unstable manifolds away from the traveling wave.

An interesting generalization would be to study parabolic PDEs formulated on $\mathbb{R}^2$ instead of on the line. For example one could study unstable nonlinear waves for conservation laws. This is an active area of research even in terms of numerical analysis of the wave profiles and their stability, as the traveling wave ansatz does not in general reduce the problem to an ODE (unless planar waves are considered). It is therefore, in general, more difficult, if not impossible, to apply dynamical systems techniques. Nevertheless it is reasonable to suggest that for any examples where the profile and unstable eigenvalues can be computed numerically, the homological equations for the jets of the parameterization could be developed and solved also numerically. This would make a very interesting topic for a future study.

Finally, we mention that in recent years a number of researchers have developed computer assisted methods of proof for studying existence questions for traveling wave solutions [92, 88, 93, 94] and also computer aided methods for verifying both existence and stability properties of such waves [95, 96, 97, 98, 99]. If one were to develop analogous computer assisted methods of proof for studying the homological equations, this would open the way to validated computation of unstable manifolds for traveling waves. Indeed such techniques would be a first step toward computer assisted proofs for connecting orbits in the full PDE (posed on the line), though several other components would be needed as well, namely, computer assisted analysis of the stable manifold and computer assisted techniques for rigorous integration of the flow. This is an ambitious program whose completion could take years of sustained research.

Acknowledgments. The authors offer sincere thanks to two anonymous referees for carefully reading an earlier version of the work. Their many suggestions greatly improved the final

manuscript. We would like to thank Christian Reinhardt for invaluable conversations and for bringing the first two authors together on this project. We thank Björn Sandstede for making us aware of the explicit eigenvalue-eigenvector pair for the scalar Nagumo equation.

REFERENCES

[1] E. J. Doedel, T. F. Fairgrieve, B. Sandstede, A. R. Champneys, Y. A. Kuznetsov, and X. Wang, *Auto-07p: Continuation and Bifurcation Software for Ordinary Differential Equations*, Technical report, 2007.

[2] B. Deconinck, F. Kiyak, J. D. Carter, and J. N. Kutz, *SpectrUW: A laboratory for the numerical exploration of spectra of linear operators*, Math. Comput. Simulation, 74 (2007), pp. 370–378.

[3] T. Rees and A. Monahan, *A general numerical method for analyzing the linear stability of stratified parallel shear flows*, J. Atmos. Ocean. Technol., 31 (2014), pp. 2795–2808.

[4] P. Brodtkorb, P. Johannesson, G. Lindgren, I. Rychlik, J. Ryden, and E. Sjo, *WAFO - A MATLAB toolbox for analysis of random waves and loads*, Proceedings of the Tenth International Offshore and Polar Engineering Conference, International Socidety of Offshore and Polar Engineers, Cupertino, CA, 3 (2000), pp. 343–350.

[5] B. Barker, J. Humpherys, J. Lytle, and K. Zumbrun, *STABLAB: A MATLAB-based Numerical Library for Evans Function Computation*, https://github.com/nonlinear-waves/stablab.git.

[6] X. Cabré, E. Fontich, and R. de la Llave, *The parameterization method for invariant manifolds.* I. *Manifolds associated to non-resonant subspaces*, Indiana Univ. Math. J., 52 (2003), pp. 283–328.

[7] X. Cabré, E. Fontich, and R. de la Llave, *The parameterization method for invariant manifolds.* II. *Regularity with respect to parameters*, Indiana Univ. Math. J., 52 (2003), pp. 329–360.

[8] X. Cabré, E. Fontich, and R. de la Llave, *The parameterization method for invariant manifolds.* III. *Overview and applications*, J. Differential Equations, 218 (2005), pp. 444–515.

[9] A. Haro and R. de la Llave, *A parameterization method for the computation of invariant tori and their whiskers in quasi-periodic maps: Explorations and mechanisms for the breakdown of hyperbolicity*, SIAM J. Appl. Dyn. Syst., 6 (2007), pp. 142–207.

[10] À. Haro and R. de la Llave, *A parameterization method for the computation of invariant tori and their whiskers in quasi-periodic maps: Numerical algorithms*, Discrete Contin. Dyn. Syst. Ser. B, 6 (2006), pp. 1261–1300.

[11] A. Haro and R. de la Llave, *A parameterization method for the computation of invariant tori and their whiskers in quasi-periodic maps: Rigorous results*, J. Differential Equations, 228 (2006), pp. 530–579.

[12] M. Canadell and À. Haro, *Computation of quasi-periodic normally hyperbolic invariant tori: Algorithms, numerical explorations and mechanisms of breakdown*, J. Nonlinear Sci., 27 (2017), pp. 1829–1868.

[13] M. Canadell and À. Haro, *Parameterization method for computing quasi-periodic reducible normally hyperbolic invariant tori*, in Advances in Differential Equations and Applications, SEMA SIMAI Springer Ser. 4, Springer, Cham, Switzerland, 2014, pp. 85–94.

[14] R. C. Calleja, A. Celletti, and R. de la Llave, *A KAM theory for conformally symplectic systems: Efficient algorithms and their validation*, J. Differential Equations, 255 (2013), pp. 978–1049.

[15] G. Huguet, R. de la Llave, and Y. Sire, *Computation of whiskered invariant tori and their associated manifolds: New fast algorithms*, Discrete Contin. Dyn. Syst., 32 (2012), pp. 1309–1353.

[16] E. Fontich, R. de la Llave, and Y. Sire, *A method for the study of whiskered quasi-periodic and almost-periodic solutions in finite and infinite dimensional Hamiltonian systems*, Electron. Res. Announc. Math. Sci., 16 (2009), pp. 9–22.

[17] X. He and R. de la Llave, *Construction of quasi-periodic solutions of state-dependent delay differential equations by the parameterization method* I*: Finitely differentiable, hyperbolic case*, J. Dynam. Differential Equations, 29 (2017), pp. 1503–1517.

[18] X. He and R. de la Llave, *Construction of quasi-periodic solutions of state-dependent delay differential equations by the parameterization method* II*: Analytic case*, J. Differential Equations, 261 (2016), pp. 2068–2108.

[19] A. Guillamon and G. Huguet, *A computational and geometric approach to phase resetting curves and surfaces*, SIAM J. Appl. Dyn. Syst., 8 (2009), pp. 1005–1042.
[20] G. Huguet and R. de la Llave, *Computation of limit cycles and their isochrons: Fast algorithms and their convergence*, SIAM J. Appl. Dyn. Syst., 12 (2013), pp. 1763–1802.
[21] J. Rinzel and G. Huguet, *Nonlinear dynamics of neuronal excitability, oscillations, and coincidence detection*, Comm. Pure Appl. Math., 66 (2013), pp. 1464–1494.
[22] R. Castelli, J.-P. Lessard, and J. D. Mireles James, *Parameterization of invariant manifolds for periodic orbits* I*: Efficient numerics via the Floquet normal form*, SIAM J. Appl. Dyn. Syst., 14 (2015), pp. 132–167.
[23] J. D. Mireles James and M. Murray, *Chebyshev-Taylor parameterization of stable/unstable manifolds for periodic orbits: Implementation and applications*, Internat. J. Bifur. Chaos Appl. Sci. Engrg., 27 (2017), 1730050.
[24] À. Haro, M. Canadell, J.-L. Figueras, A. Luque, and J.-M. Mondelo, *The Parameterization Method for Invariant Manifolds*, Applied Mathematical Sciences 195, Springer, Cham, Switzerland, 2016.
[25] C. M. Groothedde and J. D. Mireles James, *Parameterization method for unstable manifolds of delay differential equations*, J. Comput. Dyn., 4 (2017), pp. 21–70.
[26] C. Reinhardt and J. D. Mireles James, *Fourier-Taylor parameterization of unstable manifolds for parabolic partial differential equations: Formalism, implementation and rigorous validation*, Indag. Math. (N.S.), 30 (2019), pp. 39–80.
[27] J. Gonzalez, N. Tuncer, and J. D. Mireles James, *Finite Element Approximation of Invariant Manifolds by the Parameterization Method*, manuscript.
[28] R. Todd and J. Morgan, *Automated finite-difference time evolution code for conservation laws*, Minnesota J. Undergrad. Math., 4 (2019).
[29] G. Haller, *Homoclinic jumping in the perturbed nonlinear Schrödinger equation*, Comm. Pure Appl. Math., 52 (1999), pp. 1–47.
[30] G. Haller, G. Menon, and V. M. Rothos, *Šilnikov manifolds in coupled nonlinear Schrödinger equations*, Phys. Lett. A, 263 (1999), pp. 175–185.
[31] F. Bai, A. Spence, and A. M. Stuart, *The numerical computation of heteroclinic connections in systems of gradient partial differential equations*, SIAM J. Appl. Math., 53 (1993), pp. 743–769.
[32] F. S. Bai, A. Spence, and A. M. Stuart, *Numerical computations of coarsening in the one-dimensional Cahn-Hilliard model of phase separation*, Phys. D, 78 (1994), pp. 155–165.
[33] F. Christiansen, P. Cvitanović, and V. Putkaradze, *Spatiotemporal chaos in terms of unstable recurrent patterns*, Nonlinearity, 10 (1997), pp. 55–70.
[34] Y. Lan and P. Cvitanović, *Unstable recurrent patterns in Kuramoto-Sivashinsky dynamics*, Phys. Rev. E (3), 78 (2008), 026208.
[35] D. Viswanath and P. Cvitanović, *Stable manifolds and the transition to turbulence in pipe flow*, J. Fluid Mech., 627 (2009), pp. 215–233.
[36] P. Cvitanović, R. L. Davidchack, and E. Siminos, *On the state space geometry of the Kuramoto-Sivashinsky flow in a periodic domain*, SIAM J. Appl. Dyn. Syst., 9 (2010), pp. 1–33.
[37] J. Halcrow, J. F. Gibson, P. Cvitanović, and D. Viswanath, *Heteroclinic connections in plane Couette flow*, J. Fluid Mech., 621 (2009), pp. 365–376.
[38] C. Foias, M. S. Jolly, I. G. Kevrekidis, G. R. Sell, and E. S. Titi, *On the computation of inertial manifolds*, Phys. Lett. A, 131 (1988), pp. 433–436.
[39] M. S. Jolly, I. G. Kevrekidis, and E. S. Titi, *Approximate inertial manifolds for the Kuramoto-Sivashinsky equation: Analysis and computations*, Phys. D, 44 (1990), pp. 38–60.
[40] M. S. Jolly, *Bifurcation computations on an approximate inertial manifold for the* 2*D Navier-Stokes equations*, Phys. D, 63 (1993), pp. 8–20.
[41] M. S. Jolly, R. Rosa, and R. Temam, *Accurate computations on inertial manifolds*, SIAM J. Sci. Comput., 22 (2001), pp. 2216–2238.
[42] Y.-M. Chung and M. S. Jolly, *A unified approach to compute foliations, inertial manifolds, and tracking solutions*, Math. Comp., 84 (2015), pp. 1729–1751.
[43] A. J. Roberts, *The application of centre-manifold theory to the evolution of systems which vary slowly in space*, J. Aust. Math. Soc. Ser. B, 29 (1988), pp. 480–500.

[44] A. J. Roberts, *The utility of an invariant manifold description of the evolution of a dynamical system*, SIAM J. Math. Anal., 20 (1989), pp. 1447–1458.
[45] G. N. Mercer and A. J. Roberts, *A centre manifold description of contaminant dispersion in channels with varying flow properties*, SIAM J. Appl. Math., 50 (1990), pp. 1547–1565.
[46] X. Chen, A. J. Roberts, and J. Duan, *Centre manifolds for infinite dimensional random dynamical systems*, Dyn. Syst., 34 (2019), pp. 334–355.
[47] George Haller and Sten Ponsioen, *Nonlinear normal modes and spectral submanifolds: Existence, uniqueness and use in model reduction*, Nonlinear Dynam., 86 (2016), pp. 1493–1534.
[48] R. Szalai, D. Ehrhardt, and G. Haller, *Nonlinear model identification and spectral submanifolds for multi-degree-of-freedom mechanical vibrations*, Proc. A., 473 (2017), 20160759.
[49] G. Haller and S. Ponsioen, *Exact model reduction by a slow-fast decomposition of nonlinear mechanical systems*, Nonlinear Dynam., 90 (2017), pp. 617–647.
[50] F. Kogelbauer and G. Haller, *Rigorous model reduction for a damped-forced nonlinear beam model: An infinite-dimensional analysis*, J. Nonlinear Sci., 28 (2018), pp. 1109–1150.
[51] T. Breunung and G. Haller, *Explicit backbone curves from spectral submanifolds of forced-damped nonlinear mechanical systems*, Proc. A., 474 (2018), 20180083.
[52] B. Krauskopf and K. Green, *Computing unstable manifolds of periodic orbits in delay differential equations*, J. Comput. Phys., 186 (2003), pp. 230–249.
[53] B. Krauskopf, K. Green, and K. Engelborghs, *From Local to Global One-Dimensional Unstable Manifolds in Delay Differential Equations*, in EQUADIFF 2003, World Scientific, Hackensack, NJ, 2005, pp. 175–180.
[54] P. Collins and B. Krauskopf, *Chaotic Lasers: Manifolds, Bifurcations and Symbolic Dynamics*, in EQUADIFF 2003, World Scientific, Hackensack, NJ, 2005, pp. 871–876.
[55] K. Green, B. Krauskopf, and K. Engelborghs, *One-dimensional unstable eigenfunction and manifold computations in delay differential equations*, J. Comput. Phys., 197 (2004), pp. 86–98.
[56] R. C. Calleja, A. R. Humphries, and B. Krauskopf, *Resonance phenomena in a scalar delay differential equation with two state-dependent delays*, SIAM J. Appl. Dyn. Syst., 16 (2017), pp. 1474–1513.
[57] M. Dellnitz, M. Hessel-Von Molo, and A. Ziessler, *On the computation of attractors for delay differential equations*, J. Comput. Dyn., 3 (2016), pp. 93–112.
[58] J. Bouwe van den Berg, J. D. Mireles James, and C. Reinhardt, *Computing (un)stable manifolds with validated error bounds: Non-resonant and resonant spectra*, J. Nonlinear Sci., 26 (2016), pp. 1055–1095.
[59] J.-P. Lessard, J. D. Mireles James, and C. Reinhardt, *Computer assisted proof of transverse saddle-to-saddle connecting orbits for first order vector fields*, J. Dynam. Differential Equations, 26 (2014), pp. 267–313.
[60] T. Kapitula and K. Promislow, *Spectral and Dynamical Stability of Nonlinear Waves*, Applied Mathematical Sciences 185, Springer, New York, 2013.
[61] K.-J. Engel and R. Nagel, *One-parameter Semigroups for Linear Evolution Equations*, Grad. Texts in Math. 194, Springer, New York, 2000.
[62] B. Barker, *Evans Function Computation*, Master's thesis, Brigham Young University, Provo, Utah, 2009.
[63] B. Barker, J. Humpherys, G. Lyng, and J. Lytle, *Evans function computation for the stability of travelling waves*, Philos. Trans. Roy. Soc. A, 376 (2018), 20170184.
[64] B. Sandstede, *Numerical error analysis for Evans function computations: A numerical gap lemma, centered-coordinate methods, and the unreasonable effectiveness of continuous orthogonalization*, Handbook of Dynamical Systems II, Elsevier, Amsterdam, 2002, pp. 983–1055.
[65] S. Benzoni-Gavage, D. Serre, and K. Zumbrun, *Alternate Evans functions and viscous shock waves*, SIAM J. Math. Anal., 32 (2001), pp. 929–962 (electronic).
[66] T. J. Bridges and G. Derks, *The symplectic Evans matrix, and the instability of solitary waves and fronts*, Arch. Ration. Mech. Anal., 156 (2001), pp. 1–87.
[67] T. J. Bridges and G. Derks, *The symplectic Evans matrix and solitary wave instability*, in Symmetry and Perturbation Theory (Cala Gonone, 2001), World Scientific, River Edge, NJ, 2001, pp. 32–37.
[68] T. J. Bridges and G. Derks, *Constructing the symplectic Evans matrix using maximally analytic individual vectors*, Proc. Roy. Soc. Edinburgh Sect. A, 133 (2003), pp. 505–526.

[69] J. W. Evans, *Nerve axon equations.* I. *Linear approximations*, Indiana Univ. Math. J., 21 (1972), pp. 877–885.
[70] J. W. Evans, *Nerve axon equations.* II. *Stability at rest*, Indiana Univ. Math. J., 22 (1972), pp. 75–90.
[71] J. W. Evans, *Nerve axon equations.* III. *Stability of the nerve impulse*, Indiana Univ. Math. J., 22 (1972), pp. 577–593.
[72] J. W. Evans, *Nerve axon equations.* IV. *The stable and the unstable impulse*, Indiana Univ. Math. J., 24 (1975), pp. 1169–1190.
[73] J. W. Evans and J. A. Feroe, *Traveling waves of infinitely many pulses in nerve equations*, Math. Biosci., 37 (1977), pp. 23–50.
[74] A. Ghazaryan, S. Lafortune, and V. Manukian, *Stability of front solutions in a model for a surfactant driven flow on an inclined plane*, Phys. D, 307 (2015), pp. 1–13.
[75] G. N. Mercer, H. S. Sidhu, R. O. Weber, and V. Gubernov, *Evans function stability of combustion waves*, SIAM J. Appl. Math., 63 (2003), pp. 1259–1275.
[76] P. Howard and K. Zumbrun, *The Evans function and stability criteria for degenerate viscous shock waves*, Discrete Contin. Dyn. Syst., 10 (2004), pp. 837–855.
[77] J. Humpherys, B. Sandstede, and K. Zumbrun, *Efficient computation of analytic bases in Evans function analysis of large systems*, Numer. Math., 103 (2006), pp. 631–642.
[78] T. Kapitula and B. Sandstede, *Edge bifurcations for near integrable systems via Evans function techniques*, SIAM J. Math. Anal., 33 (2002), pp. 1117–1143.
[79] S. Lafortune, J. Lega, and S. Madrid, *Instability of local deformations of an elastic rod: Numerical evaluation of the Evans function*, SIAM J. Appl. Math., 71 (2011), pp. 1653–1672.
[80] M. Oh and K. Zumbrun, *Stability of periodic solutions of conservation laws with viscosity: Analysis of the Evans function*, Arch. Ration. Mech. Anal., 166 (2003), pp. 99–166.
[81] M. Oh and B. Sandstede, *Evans functions for periodic waves on infinite cylindrical domains*, J. Differential Equations, 248 (2010), pp. 544–555.
[82] R. Plaza and K. Zumbrun, *An Evans function approach to spectral stability of small-amplitude shock profiles*, Discrete Contin. Dyn. Syst., 10 (2004), pp. 885–924.
[83] T. Kapitula, N. Kutz, and B. Sandstede, *The Evans function for nonlocal equations*, Indiana Univ. Math. J., 53 (2004), pp. 1095–1126.
[84] B. Sandstede and A. Scheel, *Evans function and blow-up methods in critical eigenvalue problems*, Discrete Contin. Dyn. Syst., 10 (2004), pp. 941–964.
[85] B. Sandstede, *Evans functions and nonlinear stability of traveling waves in neuronal network models*, Internat. J. Bifur. Chaos, 17 (2007), pp. 2693–2704.
[86] P. Gray and S. K. Scott, *Autocatalytic reactions in the isothermal, continuous stirred tank reactor: Oscillations and instabilities in the system* $A + 2B \to 3B, B \to C$, Chem. Engrg. Sci, 39 (1984), pp. 1087–1097.
[87] J. K. Hale, L. A. Peletier, and W. C. Troy, *Exact homoclinic and heteroclinic solutions of the Gray-Scott model for autocatalysis*, SIAM J. Appl. Math, 61 (2000), pp. 102–130.
[88] J. Bouwe van den Berg, J. D. Mireles-James, J.-P. Lessard, and K. Mischaikow, *Rigorous numerics for symmetric connecting orbits: Even homoclinics of the Gray-Scott equation*, SIAM J. Math. Anal,, 43 (2011), pp. 1557–1594.
[89] A. Doelman, R. A. Gardner, and T. J. Kaper, *Stability analysis of singular patterns in the* $1D$ *Gray-Scott model: A matched asymptotics approach*, Phys. D, 122 (1998), pp. 1–36.
[90] P. C. Chang, *Modulation Stability of Oscillatory Pulse Solutions of the Parameterically-Forced Nonlinear Schrödinger Equation*, Master's thesis, Simon Fraser University, Vancover, CA, 2001.
[91] M. Breden, J.-P. Lessard, and J. D. Mireles James, *Computation of maximal local (un)stable manifold patches by the parameterization method*, Indag. Math. (N.S.), 27 (2016), pp. 340–367.
[92] O. Fogelklou, W. Tucker, and G. Kreiss, *A computer-assisted proof of the existence of traveling wave solutions to the scalar Euler equations with artificial viscosity*, NoDEA Nonlinear Differential Equations Appl., 19 (2012), pp. 97–131.
[93] J. Bouwe van den Berg, A. Deschênes, J.-P. Lessard, and J. D. Mireles James, *Stationary coexistence of hexagons and rolls via rigorous computations*, SIAM J. Appl. Dyn. Syst., 14 (2015), pp. 942–979.

[94] I. Balázs, J. Bouwe van den Berg, J. Courtois, J. Dudás, J.-P. Lessard, A. Vörös-Kiss, J. F. Williams, and X. Y. Yin, *Computer-assisted proofs for radially symmetric solutions of PDEs*, J. Comput. Dyn., 5 (2018), pp. 61–80.
[95] B. Barker, *Numerical Proof of Stability of Roll Waves in the Small-Amplitude Limit for Inclined Thin Film Flow*, Ph.D. thesis, Indiana University, Bloomington, IN, 2014.
[96] B. Barker, *Numerical proof of stability of roll waves in the small-amplitude limit for inclined thin film flow*, J. Differential Equations, 257 (2014), pp. 2950–2983.
[97] G. Arioli and H. Koch, *Existence and stability of traveling pulse solutions of the FitzHugh-Nagumo equation*, Nonlinear Anal., 113 (2015), pp. 51–70.
[98] B. Barker and K. Zumbrun, *Numerical proof of stability of viscous shock profiles*, Math. Models Methods Appl. Sci., 26 (2016), pp. 2451–2469.
[99] M. Creek, R. Donninger, W. Schlag, and S. Snelson, *Linear stability of the Skyrmion*, Int. Math. Res. Not. IMRN, 2017 (2017), pp. 2497–2537.